Nanoscale Advances

ROYAL SOCIETY OF CHEMISTRY

REVIEW

View Article Online
View Journal | View Issue

Open Access Article. Published on 30 July 2021. Downloaded on 2/11/2026 5:52:39 PM.
This article is licensed under a Creative Commons Attribution 3.0 Unported Licence.

Check for updates

Cite this: *Nanoscale Adv.*, 2021, **3**, 5222

High-rate transition metal-based cathode materials for battery-supercapacitor hybrid devices

Cong Wang,† Zehao Song,† Pei Shi, Lin Lv, Houzhao Wan,* Li Tao, Jun Zhang, Hanbin Wang and Hao Wang*

With the rapid development of portable electronic devices, electric vehicles and large-scale grid energy storage devices, there is a need to enhance the specific energy density and specific power density of related electrochemical devices to meet the fast-growing requirements of energy storage. Battery-supercapacitor hybrid devices (BSHDs), combining the high-energy-density feature of batteries and the high-power-density properties of supercapacitors, have attracted mass attention in terms of energy storage. However, the electrochemical performances of cathode materials for BSHDs are severely limited by poor electrical conductivity and ion transport kinetics. As the rich redox reactions induced by transition metal compounds are able to offer high specific capacity, they are an ideal choice of cathode materials. Therefore, this paper reviews the currently advanced progress of transition metal compound-based cathodes with high-rate performance in BSHDs. We discuss some efficient strategies of enhancing the rate performance of transition metal compounds, including developing intrinsic electrode materials with high conductivity and fast ion transport; modifying materials, such as inserting defects and doping; building composite structures and 3D nano-array structures; interfacial engineering and catalytic effects. Finally, some suggestions are proposed for the potential development of cathodes for BSHDs, which may provide a reference for significant progress in the future.

Received 30th June 2021
Accepted 30th July 2021

DOI: 10.1039/d1na00523e

rsc.li/nanoscale-advances

1. Introduction

The fast-growing economy of modern society has caused transitional consumption of primary energy sources accompanied by alarming environmental pollution, thus making it crucial to create high-performance energy conversion/storage devices.[1,2] Energy storage devices should have the ability of supporting the national grid, meeting the expected increment of the global energy demand, and also matching the expanding requirements of the transportation sector in terms of electrification, electric vehicles, *etc.*3 In the past few decades, lithium-ion batteries have been widely used as a charging power source in portable electronic devices due to their high energy density and high operating voltage. But present lithium-ion batteries are not able to meet some of the new emerging demands, such as fast charging, due to their low power

Hubei Yangtze Memory Labs, School of Microelectronics, Hubei University, Wuhan 430000, PR China. E-mail: houzhaow@hubu.edu.cn; wangh@hubu.edu.cn; nanoguy@126.com

† These authors have contributed equally to this work.

Cong Wang received her bachelor's degree from the Faculty of Physics and Mechatronics Engineering, Hubei University of Education, Wuhan, P. R. China. Since 2017, she has been a PhD candidate of the successive postgraduate-doctoral program at the Faculty of Physics and Electronic Science, Hubei University, Wuhan, P. R. China. Her doctoral topic focuses on the synthesis of transition metal selenides and their application in energy storage devices.

Zehao Song received his master's degree from the Faculty of Physics and Electronic Science, Hubei University, Wuhan, P. R. China. Currently, he works as a PhD student at the Institute of Solid State Electronics, Vienna University of Technology, Vienna, Austria. His research interests focus on photodetectors and supercapacitors and their hybrid integrated systems on chips.

© 2021 The Author(s). Published by the Royal Society of Chemistry

Open Access Article. Published on 30 July 2021. Downloaded on 2/11/2026 5:52:39 PM.
This article is licensed under a Creative Commons Attribution 3.0 Unported Licence.

density.[4–6] Supercapacitors are an ideal energy storage device because of some favourable features, including higher power density than batteries, and higher energy density than ordinary dielectric capacitors.[7] Based on the mechanism of energy storage, supercapacitors can be divided into three categories: double layer capacitors, Faraday quasi-capacitors and battery-super capacitor hybrid devices (BSHDs) (Fig. 1).[8] Among them, BSHDs attract more attention because they combine the high-energy-density feature of batteries and the high-power-density properties of supercapacitors. This should be attributed to the special structure where battery-type and capacitor-type electrode materials are applied in the cathode and anode, corresponding to the energy storage mechanism of the redox reaction and double layer, respectively (Fig. 2). Obviously, battery-type cathode materials are the key to achieving high-performance BSHDs.[9,10]

Battery-type cathodes mainly rely on transition metal compounds, such as metal oxides, hydroxides, sulfides, phosphides, *etc.*, which are capable of providing high specific capacity due to their rich redox reactions.[11] The electrochemical properties of different transition metal compounds are summarized in Table 1. Nickel oxide (NiO) has received much attention among transition metal oxides because of its excellent redox reversibility, high theoretical specific capacity (2584 F g^{-1}),[12] wide potential window and low cost.[13] But NiO has the drawbacks of poor electrical conductivity, slow ion diffusion rates and the change of volume during charge and discharge, inducing impaired rate performance and cycling stability.[14,15] Transition metal hydroxides are challenged by similar problems.[16] In contrast, transition metal sulfides are a new generation of active materials for supercapacitors. For example, cobalt sulfide has excellent electrochemical properties, high theoretical capacity, structural diversity and multiple valence states and is widely applied in electrochemistry in electrocatalysts, lithium-ion batteries, and supercapacitors.[17–19] Compared to oxygen or sulfur, phosphorus has lower electronegativity. Thus, transition metal phosphides show quasi-metallic structures and good electrical conductivity,[20] exhibiting better electrochemical response than transition metal oxides/sulfides.[21–23] However, due to the poor-electrical conductivity and slow ion transport kinetics of these materials, the poor-rate performance causes the trade-off of high power density and high energy density.

Lin Lv obtained his PhD in Microelectronics and Solid-State Electronics from the Huazhong University of Science and Technology, Wuhan, P. R. China. He is currently working as an Assistant Professor at the Faculty of Physics and Electronic Science, Hubei University, Wuhan, P. R. China. His research interests include electrocatalysis such as water splitting, oxygen reduction and carbon dioxide electroreduction, and related energy devices such as zinc-air batteries and supercapacitors.

Hanbin Wang obtained his PhD from Hubei University, Wuhan, P. R. China. Currently, he is working as a Professor at the School of Physical and Electronic Science, Hubei University, Wuhan, P. R. China. His research interests include Nano semiconductor materials and devices, and fuel cells.

Houzhao Wan is an associate professor at the Faculty of Physics and Electronic Science, Hubei University. He received his PhD degree in Microelectronics and Solid State Electronics at 2015 from the Huazhong University of Science and Technology, Wuhan, P. R. China. His research interests include energy storage materials and devices and their mechanism.

Hao Wang obtained his PhD from the Huazhong University of Science and Technology, Wuhan, P. R. China. Currently, he is working as Secretary of the Party Committee and Dean of the School of Microelectronics, Hubei University, Wuhan, P. R. China. He did two terms of postdoctoral research on nanomaterials at Peking University and The Chinese University of Hong Kong. His research interests include integrated circuits and new energy materials (advanced memory and brain-like chips, energy storage cells and energy management systems, photodetectors and RF chips, and fuel cell catalysts).

Open Access Article. Published on 30 July 2021. Downloaded on 2/11/2026 5:52:39 PM.
This article is licensed under a Creative Commons Attribution 3.0 Unported Licence.

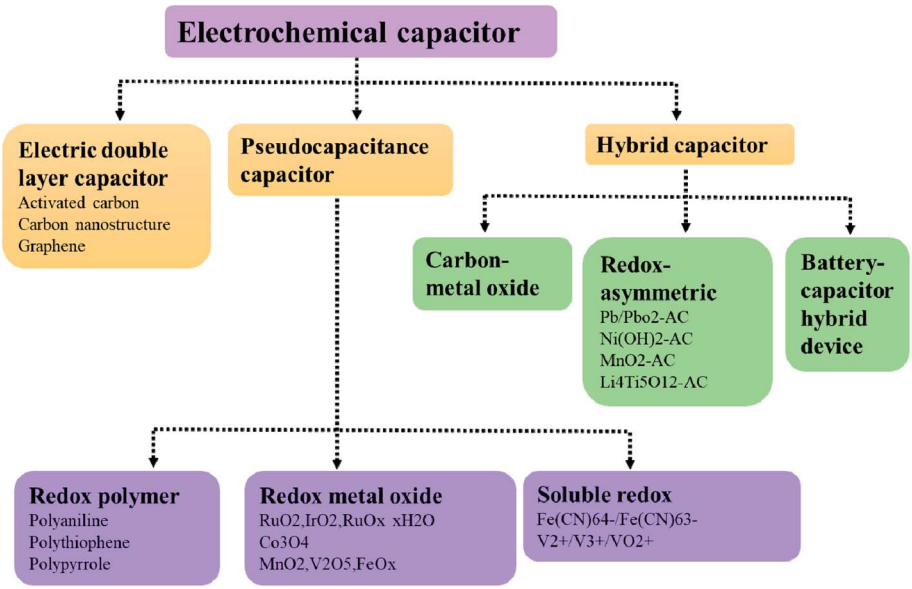

Fig. 1 Classification of electrochemical capacitors.

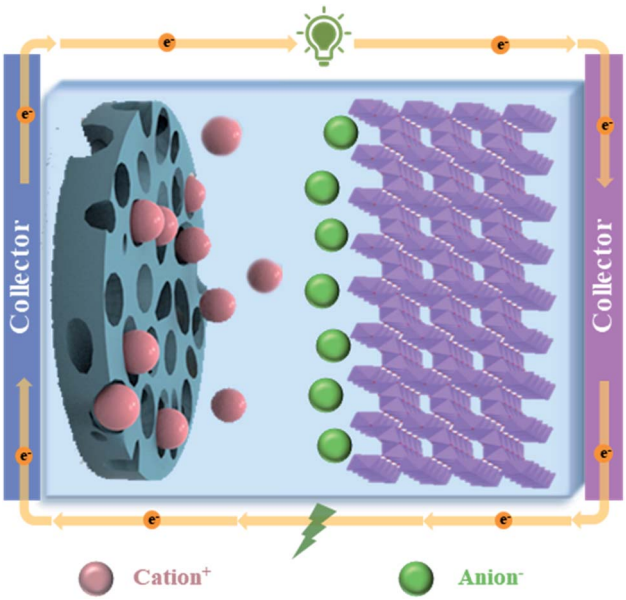

Fig. 2 Schematic diagram of the working mechanism in BSHDs.

Rate performance is an important index that characterizes the electrochemical properties of materials and devices, depending on the reversibility of redox reactions occurring on the surface and the structural stability of electrode materials.[46,47] Thus, the enhancement of rate performance is beneficial to improve the electrochemical performance of BSHDs and effectively promote their practical applications. In order to improve the rate performance of electrode materials, firstly with respect to kinetics and thermodynamics, they need to achieve high electrical conductivity and high surface activity. Secondly, some strategies such as doping, inserting defects, coupling with conducting materials, and building core–shell heterostructures can effectively improve the electrochemical activity of electrode materials and accelerate the kinetics of electrochemical reactions, thus leading to high-rate performance of electrode materials. For instance, Yu *et al.* reported urchin-like nickel–cobalt phosphide hollow spheres with polymetallic redox centers and excellent electrical conductivity, exhibiting a specific capacity of 761 C g^{-1} at a current density of 1 A g^{-1} and a capacity retention of 91.1% at 20 A g^{-1}.[48] Liu *et al.* reported composites achieved by integrating nickel–cobalt bimetallic hydroxide nanosheets with functionalized graphite.[49] The fast electron/ion transport channel enabled excellent rate performance of the composite electrode, that is, specific capacities of 2442 F g^{-1} and 2039 F g^{-1} were achieved at current densities of 1 A g^{-1} and 50 A g^{-1}, respectively, accompanied by a capacity retention of 83.5%. Cao *et al.* fabricated oxygen-rich defective Co_3O_4/graphene composites, whose oxygen vacancies on the surface can promote electrochemical charge transfer by generating another defect level in the band gap, thus significantly enhancing the rate performance of the electrode material.[50] The corresponding specific capacity was 978.1 F g^{-1} at 1 A g^{-1}, and a capacity retention of 93.7% was achieved even at 10 A g^{-1}. Although many studies have been carried out based on high-rate transition metal compound-based electrodes, they usually focus on one individual material (*e.g.* transition metal oxides), or one single property (*e.g.* porous materials), or one structure (*e.g.* hierarchically structured oxides). Nevertheless, some reviews have discussed the strategies of how to enhance the stability of transition metal compounds. Since these previous reviews have mainly focused on partial discussions, there is a need for a systematic and comprehensive review.

The purpose of this review is to provide our perspective on improving the rate performance of transition metal compound-based cathodes in BSHDs, and offer some concluding remarks and suggestions for future development, which may prove to be a reference for further research work.

 © 2021 The Author(s). Published by the Royal Society of Chemistry

Open Access Article. Published on 30 July 2021. Downloaded on 2/11/2026 5:52:39 PM.
This article is licensed under a Creative Commons Attribution 3.0 Unported Licence.

Table 1 Electrochemical properties of different types of transition metal-based compounds

Type	Electrode materials	Specific capacity ($F\ g^{-1}$) at 1 $A\ g^{-1}$	Specific capacity ($F\ g^{-1}$) at 10 $A\ g^{-1}$	Rate performance	Stability	Ref.
Oxide	NiO	473	332.8	70%	94%, $n = 3000$	24
	CoO	352	280	79.5%	92.9%, $n = 5000$	25
	Co_3O_4	1121	1023	91%	98.2%, $n = 6000$	26
	$NiCo_2O_4$	1516	1436	94.7%	93%, $n = 2000$	27
Hydroxide	$Ni(OH)_2$	2110	1171	55.5%	53%, $n = 2000$	28
	Ni Co-LDH	986.3	537.5	54.5%	92.3%, $n = 10\ 000$	29
	α-$Co(OH)_2$	1310	960	73.3%	83.9, $n = 4000$	30
	β-$Ni(OH)_2$	1065.7	812.5	76.2%	91%, $n = 10\ 000$	31
Sulfide	NiS	1315.4	677.1	51.5%	89.2%, $n = 5000$	32
	CoS	335	128	38%	87.3%, $n = 2000$	33
	CoS_2	936	746	79.7%	83%, $n = 5000$	34
	Co_9S_8	1852	1228	66.3%	86%, $n = 5000$	35
	NiCoS	1653	1344	81.3%	84%, $n = 3000$	36
	$NiCo_2S_4$	2161.7	1660	76.8%	92.4%, $n = 10\ 000$	37
Selenide	$Ni_{0.85}Se$	3150	1460	46%	90.1, $n = 5000$	38
	$Co_{0.85}Se$	1528	894.4	58.5%	92, $n = 5000$	39
	$Ni_{0.6}Co_{0.4}Se_2$	1580	1320	83.5%	90, $n = 20\ 000$	40
	$Ni_{0.67}Co_{0.33}Se_2$	784.2	674.4	86%	97%, $n = 2000$	41
Phosphide	Ni_2P	404.2	304.3	75.3%	81%, $n = 2000$	42
	$Ni_{12}P_5$	1414.4	963.4	68%	53%, $n = 1000$	43
	CoP	558	462	82.8%	98%, $n = 5000$	44
	NiCoP	1258	1056	83.9%	90.1, $n = 10\ 000$	45

2. Energy storage mechanism of high-rate electrode materials

Low electrical conductivity and ion diffusion kinetics of transition metal compounds induce a poor rate performance, which is unable to meet the requirement for high energy density. To overcome this barrier, some efficient methods of enhancing the rate performance have been established recently, including (1) finding intrinsic materials exhibiting fast electron/ion transport, (2) modifying intrinsic materials (*i.e.* inserting defects or doping), (3) building composite structures, (4) synthesizing three-dimensional (3D) designed nano-array structures, (5) interface engineering and (6) utilizing the catalytic effects of transition metal compounds (Fig. 3).

Fast electron/ion transport in intrinsic materials boosts charge transport and ion diffusion, enabling fast and reversible Faraday reactions at large current density, and thus enhancing electrochemical energy storage.[51,52] In recent years, spinel-type transition metal compound AB_2M_4 (where M is O, S) has been found to possess higher electrical conductivity and electrochemical activity than single metal oxides/sulfides, and is therefore considered a promising material for high-rate cathodes in BSHDs.[18,53–56] Specifically, high conductivity would enable rapid electron transfer, and the synergistic effect of A and B ions can provide a richer Faraday redox reaction during the charging and discharging process.[57–61] Besides the enhancement of electron transfer, the achievement of fast ion transport in the entire system is also another effective approach to improve the rate performance of electrode materials. One of the corresponding methods is to synthesize porous hollow nanostructures, which are able to exhibit superior performance to their bulk structure.[48,62] Because porous hollow nanostructures have more active sites than their bulk counterpart, a larger specific surface area would be used in charge storage;[48,63–65] the contact area between the electrolyte and active material would be increased and electrolyte penetration would be accelerated;[66,67] shortening the ion diffusion path, promoting the transfer efficiency of ions,[18,68,69] reducing the internal resistance, and consequently inducing higher rate performance.[62,70,71] However, most transition metal compounds are limited by slow electron and ion transport.

Modification of intrinsic materials can improve the quality of the interface between the electrode and electrolyte, and provides additional Faraday pseudocapacitance as well, thus enabling high capacity storage.[72–74] The modification methods include building defects and doping. Building defects is able to effectively break the periodic structure inside the crystal and alter the charge distribution in the surrounding, further changing the physicochemical properties of the electrode material.[75–77] Element doping will modulate the band gap and the conductivity of electrode materials, thus reinforcing the rate performance.[78–81] In addition, modification can reconfigure the crystalline structure inside the electrode material, which would work as a buffer, avoiding the capacity loss caused by volume expansion of electrode materials during a fast charging and discharging process.[31]

Composite structures can effectively combine the advantages of different materials to meet the demand of high rate performance. For transition metal compounds, many previous research studies have demonstrated an efficient approach of improving rate performance *via* coupling carbon-based materials. Among such carbon-based materials, graphene is one of the most widely applied, owing to its excellent electrical conductivity and huge specific surface area. Such composites would take their advantages (such as the synergistic effect from

Open Access Article. Published on 30 July 2021. Downloaded on 2/11/2026 5:52:39 PM.
This article is licensed under a Creative Commons Attribution 3.0 Unported Licence.

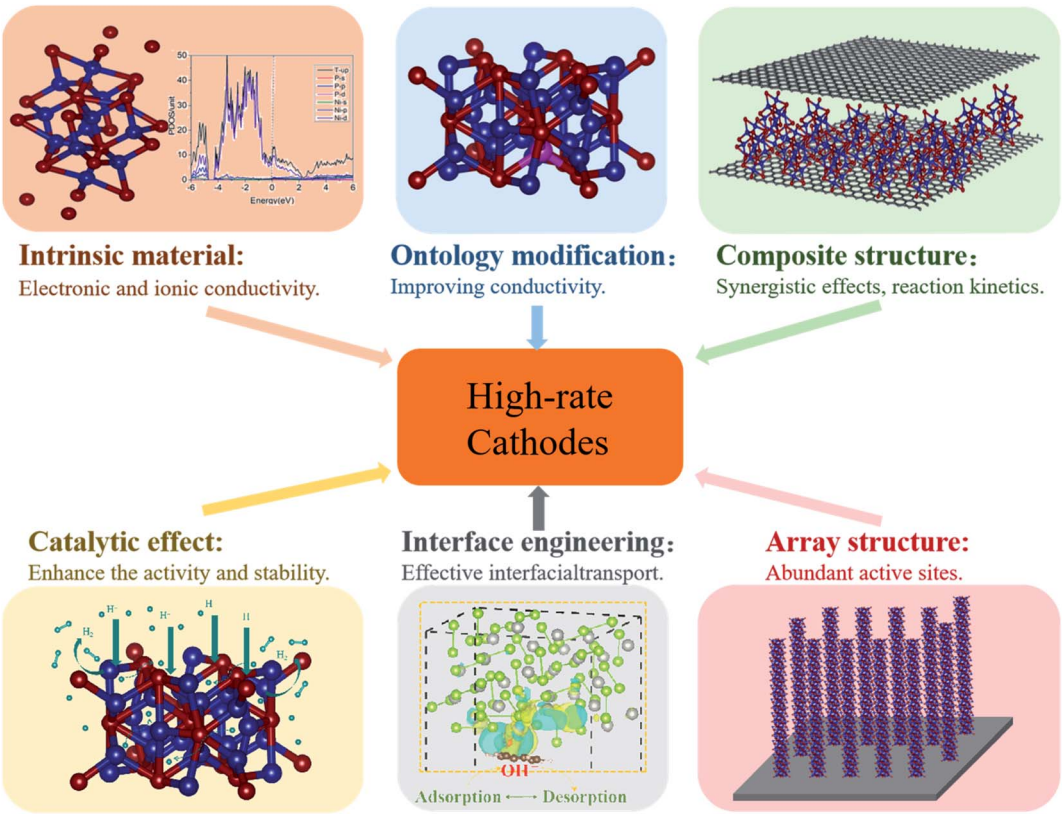

Fig. 3 Methods of enhancing the rate performance of transition metal compounds.

components and fast electron transport) to accelerate the speed of charge transfer and ion diffusion,[19,47,82,83] mitigating the volume expansion during the redox reaction.[56,84–86] Therefore, they are able to greatly enhance the rate performance of electrode materials with the improvement of cycling stability.[87,88] Another approach of optimizing energy storage performance is to build heterojunctions using different transition metal compounds (such as Co_3O_4–RuO_2,[89] and $MoSe_2$–$Ni(OH)_2$ (ref. 70)), which will provide a built-in electric field to facilitate the transfer of electrons by an electrostatic force, finally improving the kinetics of the redox reaction during charging and discharging, and thus achieving high rate performance.[90]

3D nano-array structures can utilize active materials as much as possible and provide rich redox reaction sites, further increasing the rate performance. As the quality of the electron transporting channel is crucial to the performance of electrode materials, the morphologies of 3D nanostructures would play an important role in achieving high-performance electrode materials.[91] It has been demonstrated that 3D nano-array structures consisting of 1D nanorods and 2D nanosheets have huge potential in enhancing the electrochemical properties of electrode materials. 2D nanosheets exhibit an enormous surface area, which will provide abundant active sites for redox reactions, whereas 1D nanorods have a large contact area with electrolyte ions during the electrochemical reactions. Besides, 1D nanorods not only act as an electronic highway to transfer electrons from the active material to the external circuit, but also have the ability of mitigating volume expansion.

The interface is an important position where electrochemical reactions occur in energy storage devices, and the performance of BSHD electrode materials strongly relies on effective electron and ion transport on the surface. The construction of high-quality interfaces inside composite electrodes or between the electrode/electrolyte is a key step of enhancing the electrochemical energy storage performance.[92] In addition, catalyst materials play a crucial role in redox reactions that occur during the storage and conversion of electrochemical energy. The activity and stability of catalyst materials determine the electrochemical performance of energy storage devices, more or less. Therefore, it is important to survey the catalytic characteristics of electrode materials improving the rate performance and cycling stability.

Here, we will carry out a more detailed discussion with respect to individual strategies from the above arguments. Fig. 4 summarizes the rate performance of some transition metal compound cathodes based on different strategies.

3. Strategies of enhancing the rate performance of transition metal compound-based cathodes

3.1 Intrinsic materials

3.1.1 High-conductivity electrode materials. Common battery-type transition metal compounds, such as nickel oxide,[93] cobalt oxide,[25,94] nickel sulfide,[95,96] and cobalt

 © 2021 The Author(s). Published by the Royal Society of Chemistry

Open Access Article. Published on 30 July 2021. Downloaded on 2/11/2026 5:52:39 PM.
This article is licensed under a Creative Commons Attribution 3.0 Unported Licence.

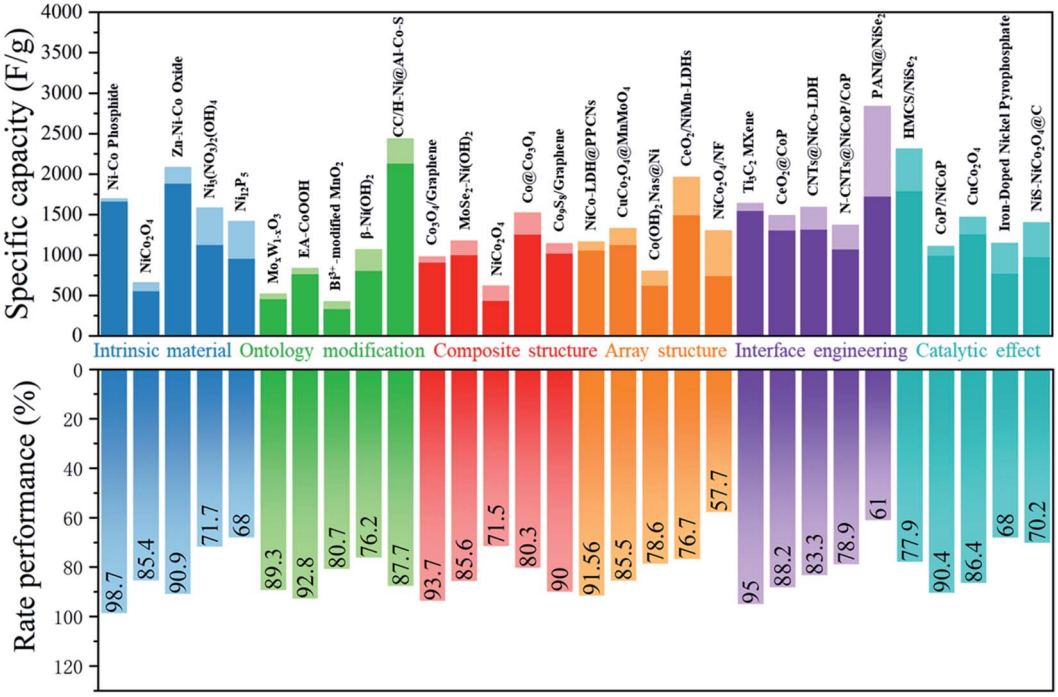

Fig. 4 Effective methods used in increasing the rate performance of transition metal based cathodes in BSHDs.

phosphide,[97] used as cathode materials usually have poor electrical conductivity, slow ion diffusion, and bad cycling stability, thus inducing low rate performance. Such transition metal compounds with low rate performance are not able to meet the needs and greatly limit practical applications.[98] Therefore, researchers have dedicated themselves to find strategies of synthesizing high conductivity electrode materials, which can make electrons transfer from the collector to the surface of the electrode material faster, consequently reducing the charge transfer resistance.[99] Among a lot of bimetallic compounds, nickel–cobalt bimetallic oxides are one of the most promising materials for high-performance pseudocapacitive electrodes. Compared to monometallic oxides, such as nickel oxide and cobalt oxide, spinel structure-based nickel–cobalt bimetallic oxides are able to offer more abundant redox active centers due to the synergistic effect, and thus higher specific capacity.[54] Jiang *et al.* prepared $NiCo_2O_4$ and used it as an electrode material, which also showed high conductivity enabling excellent rate performance and cycling stability. It has a specific capacity of 658 F g^{-1} at a current density of 1 A g^{-1}, and still kept 78% capacity retention even when the current density was increased 20 times.[61] Lin *et al.* prepared a $NiCo_2S_4$ electrode material effectively improving the interaction between the electrolyte and active material, accelerating electron transfer during charge and discharge, and thus exhibiting impressive capacity and rate performance (*i.e.* a capacity of 82.6 mA h g^{-1} at 1 A g^{-1} and even a capacity of 46.2 mA h g^{-1} at 16 A g^{-1}).[18]

With the electronegativity of the atom P in transition metal compounds being lower than that of the atoms O and S, transition metal phosphides have faster electron transfer and more active redox reactions enabling better electrochemical properties.[98] Further, larger ionic gaps in the atomic structure of transition metal phosphides would enable more efficient electron/ion transport and better electrical conductivity, and thus transition metal phosphides would have good prospects as cathode materials in BSHDs. Wang *et al.* successfully synthesized high conductivity $Ni_{12}P_5$ nanowires by a simple one-step hydrothermal method. Such $Ni_{12}P_5$ nanowires can provide abundant electrochemical active centers and excellent electron transport paths.[43] The electrode material showed a reversible specific capacity of 707.2 C g^{-1} at 1 A g^{-1} and a specific capacity of 481.7 C g^{-1} at 10 A g^{-1} with good capacity retention. Fig. 5a illustrates the crystal structure of $Ni_{12}P_5$, wherein the high porosity enables a high conductivity of 10 S cm^{-1}. Fig. 5b demonstrates the density of states of Ni and P, suggesting that the energy bands of $Ni_{12}P_5$ are mainly attributed to Ni_{2p} and P_{2p}. The partial overlap of electron densities on the Fermi energy level further confirms the high conductivity of $Ni_{12}P_5$, which is the reason for high-rate performance. Fig. 5c shows the mechanism of electron transport in $Ni_{12}P_5$ nanowires in which the adsorption/desorption of OH^- on the surface of the $Ni_{12}P_5$ nanowires promotes electron transfer; the corresponding redox reaction on the surface of the $Ni_{12}P_5$ nanowires follows eqn (1):

$$Ni_{12}P_5 + xOH^- \leftrightarrow Ni_{12}P_5(OH)_x + xe^- \quad (1)$$

3.1.2 Highly-active-site electrode materials. To improve the rate performance of transition metal compound-based cathodes in BSHDs, another effective strategy is to prepare nanostructures with highly active sites. One of the simple approaches is to transform the bulk into porous nano-hollow structures,

Open Access Article. Published on 30 July 2021. Downloaded on 2/11/2026 5:52:39 PM.
This article is licensed under a Creative Commons Attribution 3.0 Unported Licence.

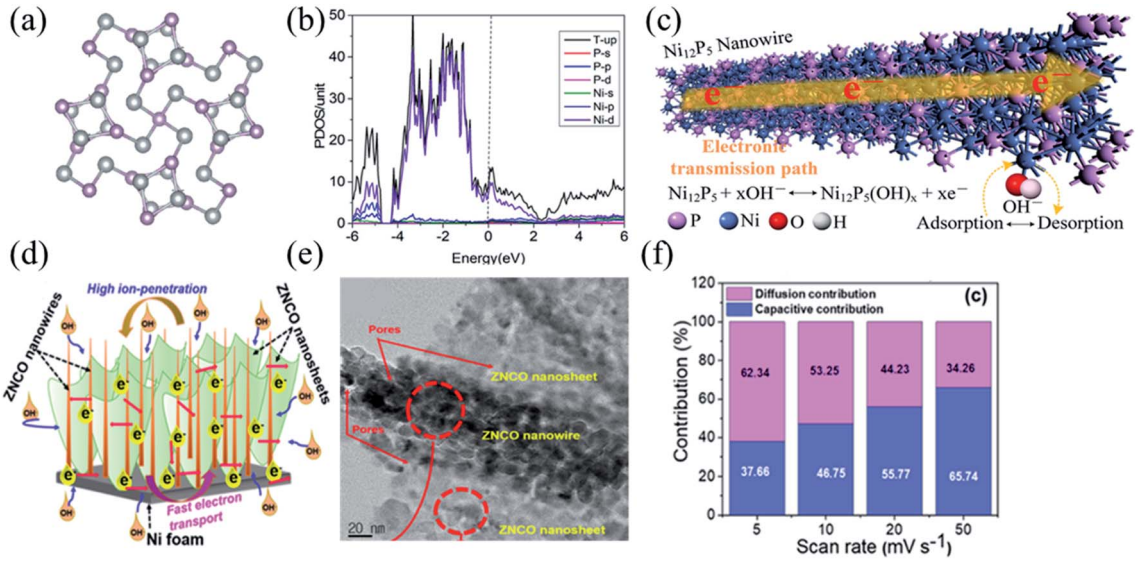

Fig. 5 (a) The crystal structure of $Ni_{12}P_5$. (b) The projected density of states of the $Ni_{12}P_5$ bulk counterpart. (c) Electron transporting mechanism of $Ni_{12}P_5$ nanowires. Panel a–c adapted with permission from ref. 43, copyright 2019, Elsevier. (d) Electron transporting mechanism of ZNCO nanostructures. (e) The HRTEM image of the ZNCO. (f) Contribution of the capacitive- and diffusion-controlled process for the ZNCO electrode at different scanning rates. Panels d–f adapted with permission from ref. 112, copyright 2020, American Chemical Society.

which would enable superior physical and chemical properties to the bulk materials.[48,62] Hollow nanostructures can facilitate penetration of the electrolyte into the interior of electrode materials, increasing the amount of electrochemically active sites, and providing a large specific surface area for charge storage.[60,61,100] Further, the large specific surface area would shorten the transport paths of ions and electrons, reducing the internal resistance, and thus enhancing the rate performance of the electrode material.[91,101,102] The pores in electrode materials can increase the contact area between the electrolyte and electrode, accelerating the kinetics of electrochemical reactions, and finally ensuring rapid and effective charge storage reactions.[103]

Among battery-type cathode materials, Co_3O_4 is considered a promising electrode material due to its high ideal specific capacity, good electrochemical stability and redox activity.[104,105] However, the rapid redox reaction causes severe attenuation of specific capacity during charging and discharging at large current density. To solve this problem, Sun *et al.* synthesized ultrathin Co_3O_4 nanosheets with high electrochemical activity and stability based on Co-MOFs as precursors.[26] The corresponding specific capacities were 1121 F g^{-1} at 1 A g^{-1} and 873 F g^{-1} at 25 A g^{-1} with a capacity retention of 77.9%. The Co_3O_4 nanosheets increase the contact area with the electrolyte, promoting the diffusion of ions in the electrode material, accelerating the reaction kinetics, and resulting in good specific capacity performance at high current densities.[106,107] In addition, the unique structure of Co_3O_4 nanosheets benefits the mitigation of structural collapse caused by volume changes during redox cycling, providing better reversible capacity and cycling stability.

Compared to monometallic/bimetallic compounds, ternary metal compounds have been widely used in energy storage systems because of higher electrochemical properties from the synergistic effect of multiple metal ions.[108–111] Kim *et al.* reported a unique 3D hierarchical nanostructure of zinc–nickel–cobalt ternary oxide (ZNCO) (Fig. 5e).[112] The synergistic effect between nanowires and nanosheets would provide abundant active sites for redox electrochemical reactions and reduce the volume expansion and mechanical strain of electrode materials during long-term charge/discharge cycles (Fig. 5d). Fig. 5f illustrates the contribution from diffusion in the ZNCO electrode at different scanning rates. The ZNCO electrode exhibited ultra-high-rate performance with specific capacities of 259.8 mA h g^{-1} at 1 A g^{-1}, and 218 mA h g^{-1} at 50 A g^{-1} and a capacity retention of 83.9%. Qu *et al.* successfully synthesized a novel 3D-layered FeCoNi double hydroxide (FeCoNi-LDH) nanocage with excellent rate performance, grown from a cation exchange reaction with a metal–organic backbone as a template. Its corresponding specific capacity was 980 F g^{-1} at 1 A g^{-1} and the capacity maintains 93% even at a large current density of 20 A g^{-1}, indicating that FeCoNi-LDH has promising applications in energy conversion and storage.[113]

3.2 Modification

3.2.1 Vacancy defects. Most of the transition metal compounds are challenged by slow electron and ion transport. Therefore, excluding the strategies mentioned before, some other technical means have been investigated to effectively improve the rate performance of electrode materials. It has been proved that vacancy defects can promote electrochemical charge transfer achieving good conductivity and rate performance, because another additional defect level would be generated in the bandgap.[114–116] A number of fascinating state-of-the-art studies have been reported. For example, Cao *et al.*

 © 2021 The Author(s). Published by the Royal Society of Chemistry

Open Access Article. Published on 30 July 2021. Downloaded on 2/11/2026 5:52:39 PM. This article is licensed under a Creative Commons Attribution 3.0 Unported Licence.

reported ultra-small oxygen vacancy-rich Co_3O_4/graphene composites with ultra-high-rate performance. The specific capacity is able to reach 978.1 F g^{-1} at a current density of 1 A g^{-1} and the capacity retention exceeded 93.7% even at 10 A g^{-1}.[50] Zou *et al.* prepared oxygen vacancy-rich NiMn-LDH based on *in situ* oxidation by an electrodeposition method, reaching a specific capacity of 2150 F g^{-1} at a current density of 1 A g^{-1} and 1518 F g^{-1} at 10 A g^{-1}, and a capacity retention of 70.6%, and thus achieving high rate performance.[117] Feng *et al.* also used electrodeposition to obtain oxygen vacancy-rich NiCo-LDH, which exhibited a specific capacity of 1563 F g^{-1} at a current density of 1 A g^{-1}. Particularly, a capacity retention of 67% can be maintained even when applied current density was increased by a factor of 20, suggesting excellent rate performance.[118]

Qiu *et al.* activated the intrinsic electrochemical properties of $Co(OH)_2$ *via* a reverse voltage method that would trigger the phase transition from $Co(OH)_2$ to CoOOH. This resulting composition of lattice disorder and continuous cavity molecular structures would greatly facilitate the kinetics. With an abundance of defects, the reactivity of CoOOH would be higher than that of $Co(OH)_2$. The electrode material showed excellent rate performance with a specific capacity of 832 F g^{-1} at 1 A g^{-1} and a capacity retention of 78% at 200 A g^{-1}.[2] In addition, they created a special lattice vacancy β-$Ni(OH)_2$-based electrode with a unique and distinctive local lattice geometry, as shown in Fig. 6a and b. The tensile strain in the corrugated nanosheets provides an appropriate buffer for the repeated redox reactions, prolonging the lifetime of the electrode at high current densities. The corresponding specific capacity was 746 C g^{-1} at a current density of 1 A g^{-1}. Even at 30 A g^{-1}, it still had a specific capacity of 457 C g^{-1} with a capacity retention of 61%.[31] Eqn (2) explains the mechanism of this process, where oxygen vacancies and vanadium vacancies generated in the electrodes exhibit superior redox energy barriers, benefitting redox activity and reversible charge storage.

$$4Ni_{0.75}V_{0.25}(CO_3^{2-})_{0.125}(OH)_2H_2O + 2OH^- \rightarrow 3Ni(OH)_2 + VO_2 + 6H_2O + 0.5CO_3^{2-} + e^- \quad (2)$$

3.2.2 Doping. Doping can improve the capacity performance of electrode materials by modulating their conductivity.[119–121] A lot of research studies report that metal atom doping can increase the conductivity of transition metal oxides by generating additional oxygen vacancies. For example, Chen *et al.* doped Al into cobalt sulfide nanosheets by an electrodeposition method. The appropriate amount of Al doping is able to increase conductivity and enhance the electrochemical activity of cobalt sulfide, resulting in good electrochemical performance. The electrode material had a specific capacity of 2434 F g^{-1} at 1 A g^{-1}. It still had 72.3% capacity retention when current density was increased by 100 times.[122] Ni doped cobalt–cobalt nitride was prepared by Wang *et al.* which showed a specific capacity of 450 F g^{-1} at a current density of 2 mA cm^{-2} and a capacity retention of 82.5% at a current density of 50 mA cm^{-2}.[123] Wei *et al.* doped Mn into Ni–Co layered double hydroxide nanosheets coated by polyaniline-derived carbon. The Mn doping enabled a rich redox reaction (*i.e.* $Mn^{2+} \leftrightarrow Mn^{3+} \leftrightarrow Mn^{4+}$), which effectively improved the specific capacity and rate performance. A high specific capacity of 1282.06 C g^{-1} and excellent rate stability were observed at a current density of 1 A g^{-1}, and the capacity retention was 74.99% when the specific current was increased to 10 A g^{-1}.[124]

In addition to the doping of metallic elements into transition metal compounds, the doping of non-metallic elements (O, N, S, F, and P) is also able to increase conductivity.[125–127] Further, it can enable some other features, including adding the functional groups in the electrodes, improving their hydrophilicity/oil properties, and promoting the transporting efficiency of electrolyte ions.[71,78,79,81,128] Wang *et al.* doped nitrogen into cobalt phosphide nanowire arrays, which increased the conductivity of cobalt phosphide, improving charge transfer, and giving rise to the high-rate performance of cobalt phosphide. In addition, the doping of N elements increased the number of active sites of the redox reaction in cobalt phosphide, thus increasing the specific capacity. It provides a specific capacity of 232.4 mA h g^{-1} at a current density of 2 mA cm^{-2}, and maintains a capacity retention of 52% when the current density is increased to 50 mA cm^{-2}.[129] Meng *et al.* homogeneously doped P into Co–Ni–S nanosheet arrays by an electrodeposition method, which showed an ultra-high specific capacity of 3677 F g^{-1} at 1 A g^{-1} with excellent rate performance (*i.e.* a capacity retention of 63% at 20 A g^{-1}).[130] Wang *et al.* performed sulfur doping by heat treatment and obtained S-doped CoP nanotube arrays with a capacity of 610 F g^{-1} at a current density of 1.0 A g^{-1} and capacity retention of 56% at 20 A g^{-1}.[131] Yang *et al.* encapsulated Mo clusters in the holes of the Ni-MOF frame structure to improve the conductivity and stability of the Ni-MOF (Fig. 6c and d). The nanosheet structure of the Mo-doped Ni-MOF acts as a highway of charge transport, which enables faster charge transportation and the higher conductivity of the electrode material, and thus achieves excellent rate performance. The prepared Mo-doped Ni-MOF electrode exhibits a high specific capacity of 802 C g^{-1} at 1 A g^{-1}, and even a specific capacity of 480 C g^{-1} at 10 A g^{-1}.[132]

3.3 Composite structure

3.3.1 Carbon-based composite structure. Among battery-type electrode materials, NiO is widely used because of its excellent redox and charge storage properties, low cost, and environmental friendliness.[133–135] However, NiO is also challenged by poor electrical conductivity and cycling stability, which would limit practical applications. To solve this problem, an effective strategy is coupling NiO with other highly porous and conductive materials, such as graphene, activated carbon, and carbon nanotubes because such composite structures can significantly increase the conductivity and improve electrochemical properties. Graphene is a typical 2D material with in-plane carbon atoms arranged in a honeycomb pattern *via* the sp^2-bond, enabling high electrical conductivity,[136] a large specific surface area and high theoretical specific capacity.[137] In addition, its ultrathin 2D structure makes fast charge transfer

Open Access Article. Published on 30 July 2021. Downloaded on 2/11/2026 5:52:39 PM.
This article is licensed under a Creative Commons Attribution 3.0 Unported Licence.

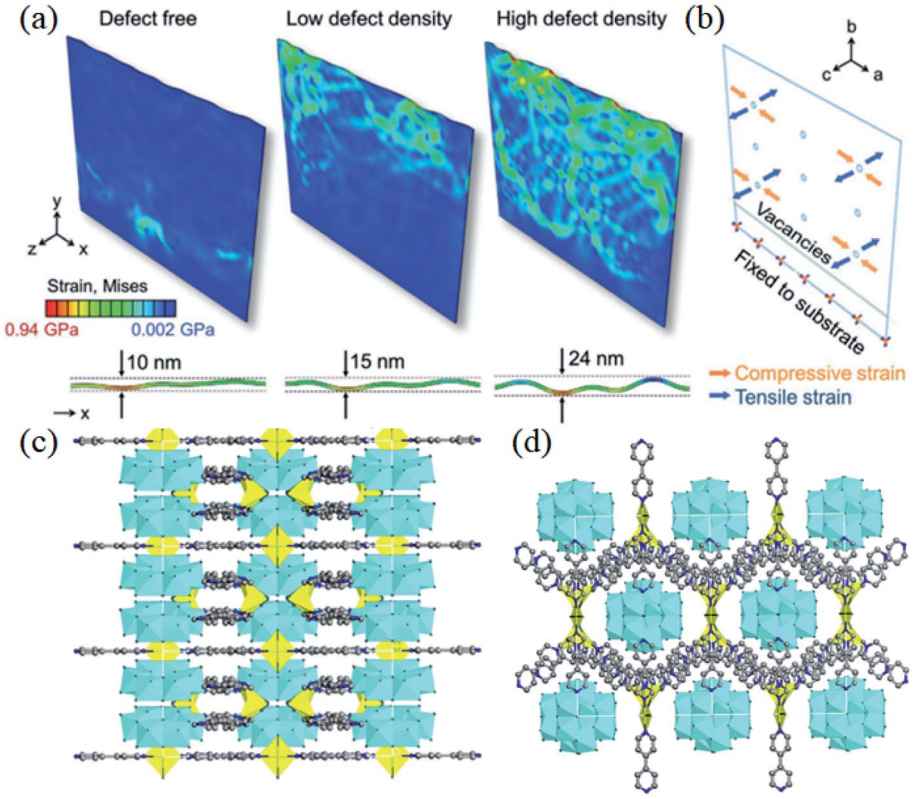

Fig. 6 (a) von Mises strain and *c*-axis displacement in nanosheets depicting the corrugation formation process for 0%, 8%, and 18% disordered regions. (b) Schematic of the strain direction on nanosheets during the phase change from α-$Ni(OH)_2$ to β-$Ni(OH)_2$. Panels a and b adapted with permission from ref. 31, copyright 2020, Wiley-VCH. (c and d) Schematic diagram of the Mo doped Ni-MOF nanosheet structure along the *a*-axis and *c*-axis. Panels c and d adapted with permission from ref. 132, copyright 2020, Elsevier.

possible in the plane, whereas its high porosity from the intra- and inter-layer enables fast ion transport.[138,139] Therefore, the combination of graphene with NiO forming some unique structures is expected to be a desired approach of enhancing the electrochemical performance of electrode materials based on the synergistic effect.[140] Wang *et al.* synthesized reduced graphene oxide@NiO (rGO@NiO) composites where NiO nanoparticles were uniformly distributed on rGO, and confirmed their ability to strengthen the accessibility from the rGO@NiO composites to the electrolyte.[141] In addition, the special structure of rGO promotes the fast electron/ion transport.[46,135] The synergistic effect of rGO and NiO endows the composite electrode with excellent rate performance with a specific capacity of 1093 F g^{-1} at a current density of 1 A g^{-1}, and 875 F g^{-1} at 10 A g^{-1} and a capacity retention of 80%.

Besides NiO, other transition metal compounds can also be coupled with carbon materials achieving high rate performance, such as $Ni(OH)_2$/RGO (1795 F g^{-1} at 1 A g^{-1}, 85.68% capacity retention at 40 A g^{-1}),[142] PEG/NiCo-DH (2442 F g^{-1} at 1 A g^{-1}, a capacity retention of 83.5% at 50 A g^{-1}),[49] $NiCo_2S_4$/PCF (1169 F g^{-1} at 1 A g^{-1}, a capacity retention of 81.3% at 20 A g^{-1}),[56] Co_9S_8/RGO (1140 F g^{-1} at 4 A g^{-1}, a capacity retention of 74.5% at 30 A g^{-1}),[19] and (Ni, Mo)S_2/RGO (2379 F g^{-1} at 1 A g^{-1}, a capacity retention of 60.5% at 100 A g^{-1}).[64] Zheng *et al.* prepared ultrathin, highly crinkled CoP/RGO nanosheet arrays *via* a hydrothermal phosphorylation method (Fig. 7a).[143] In such CoP/RGO composites, the pores in the nanosheets can serve as active sites for electrolyte diffusion and charge migration, facilitating the redox reaction process, and thus excellent electrochemical properties. Fig. 7b illustrates the partial density of states of the CoP/RGO composite determined by first principles calculations. The strong hybridization between the O atom of RGO and the Co atom of CoP suggests the existence of C–O–Co bonds between the interface of RGO and CoP.[128] Fig. 7c shows the structural model of OH^- on the surface CoP (201) and the interface CoP (201)/RGO (001), and the corresponding adsorption energy. The existence of RGO can greatly reduce the adsorption energy of OH^- on CoP, thus enhancing the electrochemical performance. The CoP/RGO electrode shows a specific capacity of 1438.0 C g^{-1} at 1 A g^{-1}, and 1198.9 C g^{-1} at 10 A g^{-1} and a capacity retention of 83.4%. Moosavifard *et al.* created graphene coated Ni_3S_2 nanocube (RGO/Ni_3S_2) composites, which can be applied in high-performance and low-cost BSHDs electrodes. RGO/Ni_3S_2 electrodes exhibit high rate performance, that is, an ultra-high specific capacity of 616 C g^{-1} at 1 A g^{-1} and a high specific capacity of 377 C g^{-1} at 10 A g^{-1}.[144]

3.3.2 Heterojunction composite structure. Building a heterojunction structure based on different electrode materials has been a hot research topic in nano/microstructure engineering,

 © 2021 The Author(s). Published by the Royal Society of Chemistry

Open Access Article. Published on 30 July 2021. Downloaded on 2/11/2026 5:52:39 PM.
This article is licensed under a Creative Commons Attribution 3.0 Unported Licence.

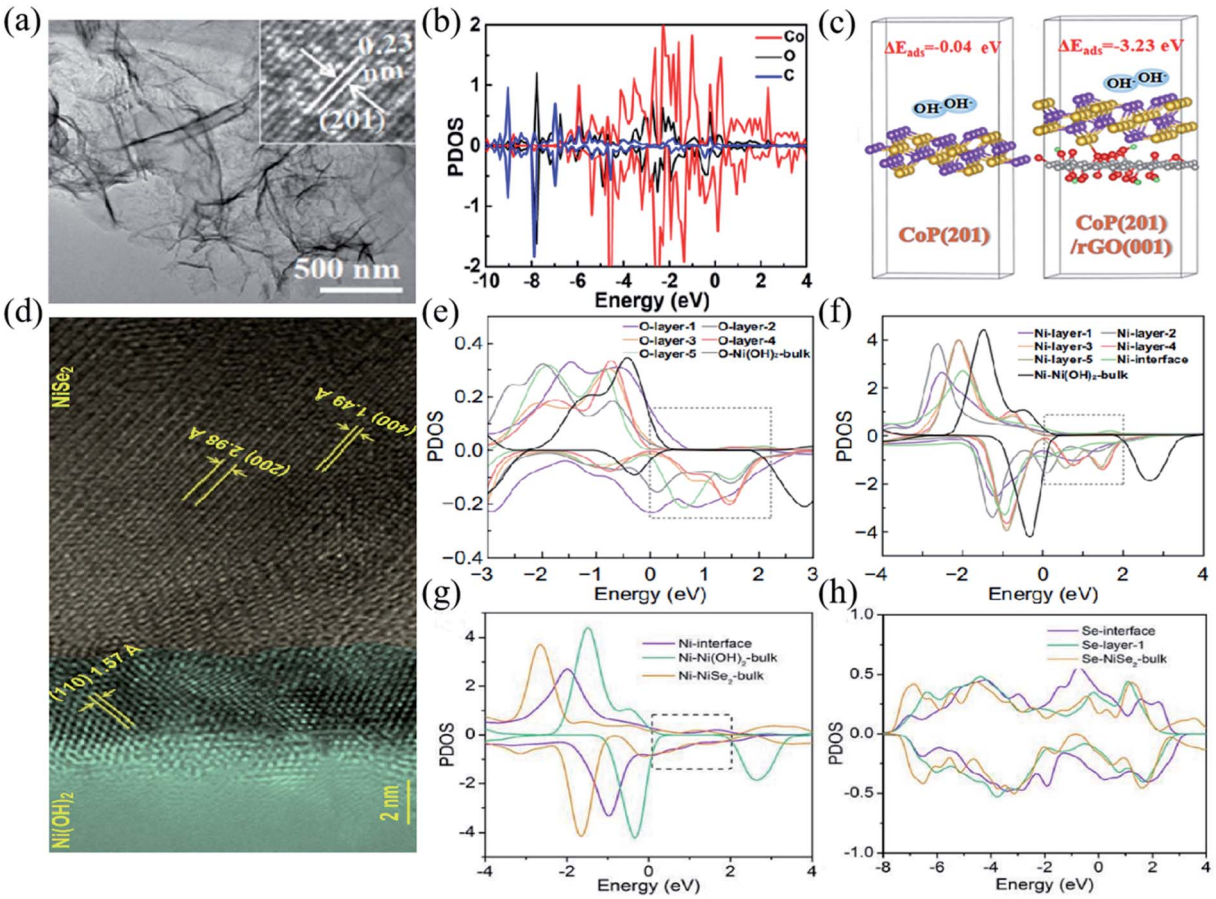

Fig. 7 (a) TEM images of the CoP/rGO nanosheets. (b) PDOS of Co, O, and C atoms in CoP (201)/rGO (001). (c) The structure models and the corresponding adsorption energies of OH^- for the CoP (201) surface and CoP (201)/rGO (001) interface. Panels a–c adapted with permission from ref. 143, copyright 2021, American Chemical Society. (d) HRTEM images of the $NiSe_2/Ni(OH)_2$ heterojunction. (e and f) PDOS of O and Ni atoms at different layers, respectively. (g) The PDOS of Ni atoms at the $Ni(OH)_2/NiSe_2$ interface, in bulk $NiSe_2$, and in bulk $Ni(OH)_2$. (h) The PDOS of Se atoms at and near the interface, as well as in the bulk. Panels d–h adapted with permission from ref. 16, copyright 2020, Springer Nature.

and is able to further optimize the energy storage performance.[145–147] With built-in fields caused by the mismatch of energy bands from different materials, electron transfer at the interface of the heterojunction would be promoted by an electrostatic force, thus improving the kinetics of redox reactions during charging and discharging.[90,148,149] Wang *et al.* prepared $MgCo_2O_4$@MnO_2 core–shell structures by growing MnO_2 nanostructures on $MgCo_2O_4$ nanoflakes, which showed excellent rate performance (*i.e.* 852.5 F g^{-1} at 1 A g^{-1}, and 573.3 F g^{-1} at 40 A g^{-1} and a capacity retention of 67.2%).[53] Sha *et al.* uniformly deposited $Ni(OH)_2$ on silicon carbide nanowires, which promoted its interaction with the electrolyte shortening the ion diffusion distance.[82] The SiC NWS@$Ni(OH)_2$ electrode material showed excellent rate performance, that is, 1724 F g^{-1} at 2 A g^{-1}, and 1412 F g^{-1} at 100 A g^{-1} and a capacity retention of 81.9%. Angaiah *et al.* synthesized molybdenum diselenide-nickel hydroxide nanohybrids with molybdenum diselenide grown on nickel hydroxide nanosheets, which was confirmed to have higher conductivity than nickel hydroxide. The rapid electron transfer that occurred at high current densities suggests improved rate performance (*i.e.* 1175 F g^{-1} at 1 A g^{-1}, and 1006 F g^{-1} at 10 A g^{-1} and a capacity retention of 85.6%).[70]

Sun *et al.* prepared (100)-$NiSe_2$/(110)-$Ni(OH)_2$ heterojunction composites using an epitaxial-like growth strategy (Fig. 7d).[16] Owing to the large specific surface area and suitable microporous structure of the $NiSe_2/Ni(OH)_2$ heterojunction, abundant electrochemically active centers would enable easy access of electrons to the electrolyte and rapid migration of ions inside the electrode. Fig. 7e–h illustrate the electronic density of states of the atoms on the $NiSe_2/Ni(OH)_2$ interface. The $NiSe_2/Ni(OH)_2$ electrode material exhibits excellent electrochemical properties with specific capacities of 909 C g^{-1} at 1 A g^{-1}, and 597 C g^{-1} at 20 A g^{-1} and a capacity retention of 63.7%. Zeng *et al.* successfully prepared $ZnCo_2O_4$@$MnCo_2O_4$ heterojunction structure nanosheets with several advantages, including a large specific surface area, good structural stability and good electrical conductivity, exhibiting high-rate performance. The corresponding specific capacity is 254 F g^{-1} at 1 A g^{-1}, and it can remains 186 F g^{-1} even at 10 A g^{-1}.[150] Li *et al.* fabricated the α-$Ni(OH)_2/NiS_{1.97}$ heterojunction by an ion-exchange based epitaxial growth method. Heterojunctions allow the components to provide ion/electron transport paths for each other, increasing the utilization rate of active materials, and thus achieving high specific capacity and rate performance. The

Open Access Article. Published on 30 July 2021. Downloaded on 2/11/2026 5:52:39 PM.
This article is licensed under a Creative Commons Attribution 3.0 Unported Licence.

corresponding specific capacity is as high as 2375.8 F g^{-1} at 1 mV s^{-1} and 939.5 F g^{-1} at 10 mV s^{-1}.[151]

3.4 Array structure

Since the quality of the electron transport channel is crucial to the performance of electrode materials, different morphologies of nanomaterials usually alter electron transporting properties by directly affecting the specific surface area and density of electrode materials.[55,91,152,153] Therefore, a reasonable design of the electrode structure plays an important role in the development of advanced electrode materials for high-performance BSHDs.[99,129,154] 3D array structures are found to increase the specific surface area and density of electrode materials, which would provide abundant electrochemical activity centers, facilitating charge transport, and consequently strengthening their electrochemical performance.[54,154–157] Therefore 3D array structures are considered attractive for maximizing the use of active materials.[158–160] Wang *et al.* prepared high-performance electrode materials by depositing arrays of copper hydroxide nanosheets on nickel grids *via* electrodeposition.[157] They have a specific capacity of 798.2 F g^{-1} at 1 A g^{-1} and a specific capacity of 556.4 F g^{-1} at 20 A g^{-1} with a capacity retention of 70%. As copper hydroxide nanosheets have a large specific surface area which can sufficiently contact the electrolyte during the charging and discharging process, the length of the ion diffusion path would be shortened and the "dead volume" in the electrode would greatly reduce. In addition, the *in situ* growth method avoids the use of polymer binders, which significantly improves electron transfer and ion diffusion.[48,68,103] Chen *et al.* reported a composite electrode consisting of a vertical, ordered arrangement of $NiCo_2S_4$ nanoflakes covered by elongated nickel columns (Fig. 8a).[161] The array structure enabled fast charge storage/transfer and promoted reaction kinetics, allowing the active materials to react efficiently. The transmission electron microscopy (TEM) image in Fig. 8b shows intersecting ultrathin $NiCo_2S_4$ sheets forming a sparse nanostructure. The contribution rate of the $NiCo_2S_4$@NC array electrode at different scan rates is shown in Fig. 8c. With the increment of the scan rate, the contribution from diffusion decreases. The shorter ion diffusion time at high scan rates results in inadequate redox reactions. In this case, the capacitive control occurring on the material surface would dominate. Due to the good charge transfer kinetics and fast electron transfer, the $NiCo_2S_4$@NC array electrode has an ultra-high specific capacity of 486.9 mA h g^{-1} at 1 A g^{-1} and 150 mA h g^{-1} even at a very high current density of 100 A g^{-1}.

Transition metal phosphides have excellent electrical conductivity and redox activity due to the lower electronegativity of phosphorus, as mentioned before.[42,44,45,162] Chen *et al. in situ* grew dense $NiCo(HPO_4)_2$–$3H_2O$ nanosheet arrays on porous CuO nanowires, referred to as Cu/p-CuO/NiCo-P, and the corresponding schematic diagram is shown in Fig. 8d.[163] Fig. 8e suggests that the single layer of $NiCo(HPO_4)_2$–$3H_2O$ consists of octahedra [(Ni–Co)O_6] and tetrahedra [PO_4]. Cu/p-CuO nanowires would increase the conductivity of the whole electrode materials as the conducting frame and provide a large specific

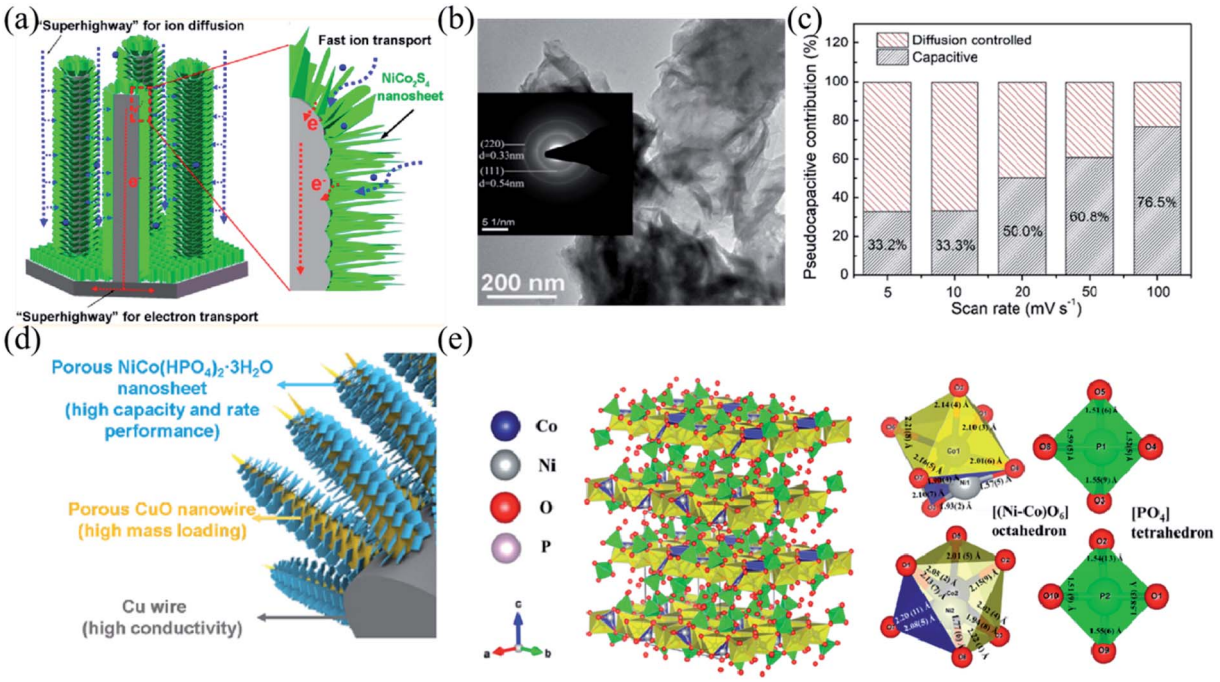

Fig. 8 (a) Schematic illustration of ion diffusion and electron transport in the vertically aligned $NiCo_2S_4$@NC-array. (b) Transmission electron microscopy image of $NiCo_2S_4$ Nanoflakes. (c) Ratio of pseudocapacitive contribution at different scan rates. Panels a–c adapted with permission from ref. 161, copyright 2020, American Chemical Society. (d) Structure advantages of the Cu/p-CuO/NiCo-P hybrid material. (e) 3D atomic configuration of a $NiCo(HPO_4)_2$–$3H_2O$ unit cell and the local coordination of the strongly distorted [(Ni–Co)O_6] octahedron and [PO_4] tetrahedron. Panels d and e adapted with permission from ref. 163, copyright 2020, American Chemical Society.

 © 2021 The Author(s). Published by the Royal Society of Chemistry

Open Access Article. Published on 30 July 2021. Downloaded on 2/11/2026 5:52:39 PM.
This article is licensed under a Creative Commons Attribution 3.0 Unported Licence.

surface area for high-quality loaded active substances. The synergistic effect of Ni and Co effectively improves the electrical conductivity and capacitive properties of NiCo-P. The abundant pores and defects of ultrathin NiCo-P nanosheets can effectively expose the active centers promoting ion diffusion and charge transfer. The Cu/p-CuO/NiCo-P electrode exhibits ultra-high specific capacity (*i.e.* 1768.5 C g^{-1} at 1 A g^{-1}) and excellent rate performance (*i.e.* 1144.8 C g^{-1} at 100 A g^{-1}, 64.7% capacity retention).

3.5 Interface engineering

Since the interface of electrode materials is an important region where electrochemical reactions occur, the capacitive performance of BSHD electrode materials strongly depends on effective electron and ion transport at the interface. Therefore, building effective interfaces inside composite electrodes or between the electrode/electrolyte is key to improving the electrochemical energy storage performance.[92] Interfaces between a metalloid/semiconductor would form Schottky contact, which can facilitate electron transfer from the free-electron-rich metalloid to the semiconductor and leave holes in the metalloid, thus enhancing OH^- adsorption.[164] In addition, the interface will release additional electrons during charging and discharging, ultimately improving the electrochemical performance of the electrode.[165,166] Such interface engineering has been verified as an effective approach of improving the conductivity and structural stability of electrodes in SBHs by many previous studies.[167–169] For example, Du *et al.* reported a $NiCo_2O_4$ nanowires/reduced graphene oxide (RGO) electrode material, which is able to combine the energy storage mechanisms of capacitive and Faraday materials.[165] With the interconnected porous skeleton of the RGO/$NiCo_2O_4$ nanocomposite and the polarization of the interface caused by the difference of work function, the kinetics of the electronic and ionic reactions are enhanced, the structural stability is improved, and the rate performance of the RGO/$NiCo_2O_4$ nanostructure is greatly enhanced, that is, 4.37 F cm^{-2} at 2 mA cm^{-2} and 2.59 F cm^{-2} at 10 mA cm^{-2} with 67.5% capacity retention. Gao *et al.* proposed a simple interface engineering strategy where 2D MoS_2 nanosheets were *in situ* integrated into a 3D polypyrrole framework *via* a DBS-anion intermediate linkage, consequently forming a novel MoS_2-DBS-PPy film.[168] As such the MoS_2-DBS-PPy film combined the excellent conductivity of PPy chains and the high specific surface area of MoS_2 nanosheets, and exhibited excellent rate performance (*i.e.* 1.2 F cm^{-2} at 0.5 mA cm^{-2}, and 0.6 F cm^{-2} at 10 mA cm^{-2} with 50% capacity retention).

With the capability of strengthening the conductivity and stability of electrode materials by forming a highly conductive layer,[170,171] polyaniline is widely implemented in energy devices by coupling with pseudocapacitive electrode materials.[172–174] Cao *et al.* synthesized V_2O_5/PANI nanomaterials *via in situ* one-step oxidative polymerization of aniline monomers, which will insert vanadium vacancies and PANI on the surface of V_2O_5 (Fig. 9a).[175] With the tilting of vanadium atoms, an unbalanced charge distribution generates in the plane, thus forming a local electric field which would provide the Coulomb force facilitating ion diffusion (Fig. 9b). Vanadium vacancies enable fast electron transfer by providing vacancy sites for electron adsorption/desorption, and also catalyze redox reactions on the

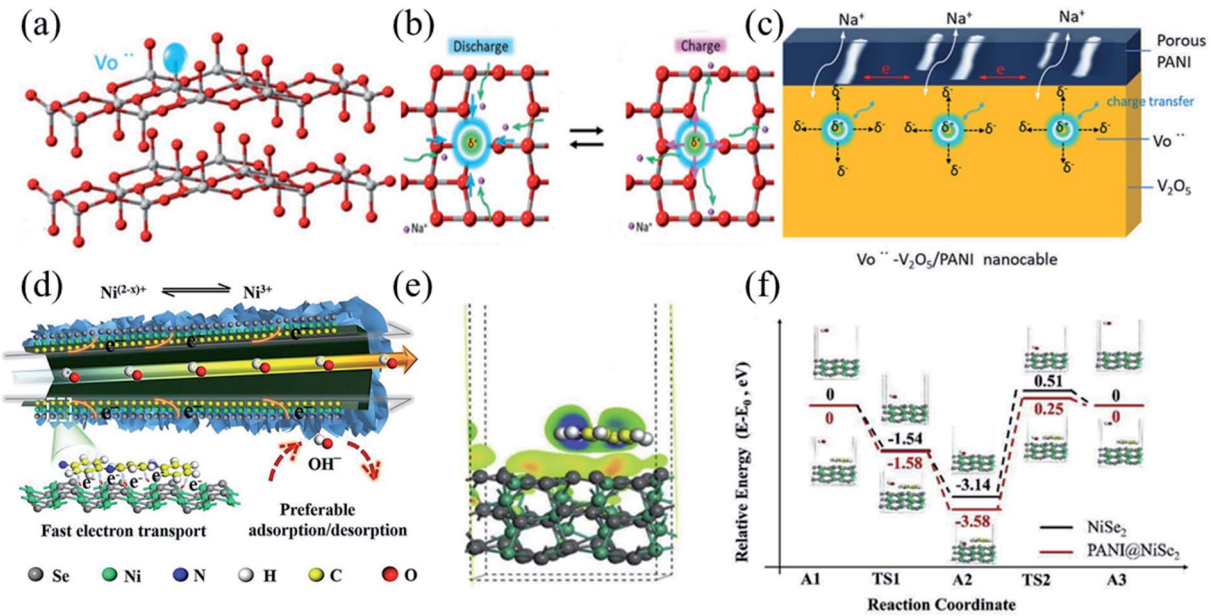

Fig. 9 (a) The vacancy site in the V_2O_5 structure. (b) Schematic illustration of charge transfer behavior around the Vö region by forming a local electric field (*E*). (c) The enhanced charge transfer kinetics mechanism of Vö–V_2O_5/PANI due to the synergy of Vö and PANI. Panels a–c adapted with permission from ref. 175, copyright 2019, WILEY-VCH. (d) The electron transport mechanism of PANI@$NiSe_2$. (e) The electronic density difference of PANI@$NiSe_2$. (f) The DFT calculations of the transition-state energy of adsorbed hydroxyl (ΔG_{OH^-}). Panels d–f adapted with permission from ref. 176, copyright 2019, Elsevier.

Open Access Article. Published on 30 July 2021. Downloaded on 2/11/2026 5:52:39 PM.
This article is licensed under a Creative Commons Attribution 3.0 Unported Licence.

surface. In addition, as an external percolation charge-transporting channel in the nanostructure, the high conductivity of the porous polyphenylene shell layer accelerates electron transport (Fig. 9c). Therefore, with vanadium vacancies and the interface modification of PANI, the charge transfer kinetics of the V_2O_5/PANI electrode would be enhanced, resulting in excellent electrochemical performance. It exhibited a specific capacity of 353.8 F g^{-1} at 1 A g^{-1} and a capacity retention of 50% at 10 A g^{-1}. Yang *et al.* fabricated a PANI/$SeNi_2$ core–shell nanotube electrode with different electron concentrations (Fig. 9d).[176] The strong interaction between PANI and $SeNi_2$ through the CNI–Se bond can induce electron accumulation at the Ni ion, which not only promotes electron transfer within the electrode, but also increases the theoretical Faraday capacity of the electrode. The Faraday redox reaction occurring at the electrode follows eqn (3):

$$\mathrm{PANI@NiSe_2} + (1 + x)\mathrm{OH^-} \leftrightarrow \mathrm{NiSe_2(OH)}_{1+x} + (1 + x)\mathrm{e^-} \quad (3)$$

Fig. 9e illustrates the transition state energy of the adsorbed hydroxyl group (ΔG_{OH^-}) calculated by DFT. Compared to $NiSe_2$, the strong interaction through the CNI–Se bridge bond at the interface of PANI/$NiSe_2$ promoted the electron transfer and the adsorption/desorption of ions on the surface, as shown in Fig. 9f. The combination of $NiSe_2$ and PANI induced electron accumulation from lower valence states or a wide range of valence changes of Ni ions, which improved the specific capacity and rate performance of the electrode material. The electrode had a specific capacity of 275.6 mA h g^{-1} at 1 A g^{-1} and a capacity retention of 61% at 10 A g^{-1}.

3.6 Catalytic effect

As catalyst materials play a crucial role in redox reactions during electrochemical energy conversion and storage,[177–179] their activity and stability would determine the electrochemical performance of energy storage devices. Thus, it makes sense to study the catalytic effect of electrode materials, further enhancing the rate performance and cycling stability of electrode materials.[180,181] Transition metal sulfides have received great attention in the application of energy conversion and storage devices due to their high specific capacity and rate performance.[182–184] Guo *et al.* prepared 3D Ni_9S_8/O–MoS_2 nanostructures used in supercapacitors and hydrogen precipitation catalysts. Ni_9S_8 nanorods acted as conducting channels of electrons in the Ni_9S_8/O–MoS_2 nanocomposites, enhancing electron transport throughout the electrodes, and thus achieved high electrochemical performance. It exhibited a specific capacity of 907 F g^{-1} at 2 A g^{-1} and retained a specific capacity of 430 F g^{-1} at 7 A g^{-1}, enabling good rate performance. In addition, the oxygen doping of MoS_2 would offer more active sites, which would participate in the catalytic process of the hydrogen precipitation reaction. Therefore, the Ni_9S_8/O–MoS_2 composites also had highly electrocatalytic properties, and can be applied for hydrogen production.[185]

Transition metal phosphides are considered a kind of stable and effective catalyst material because of their unique catalytic and electronic properties. Owing to the electron-rich metallic

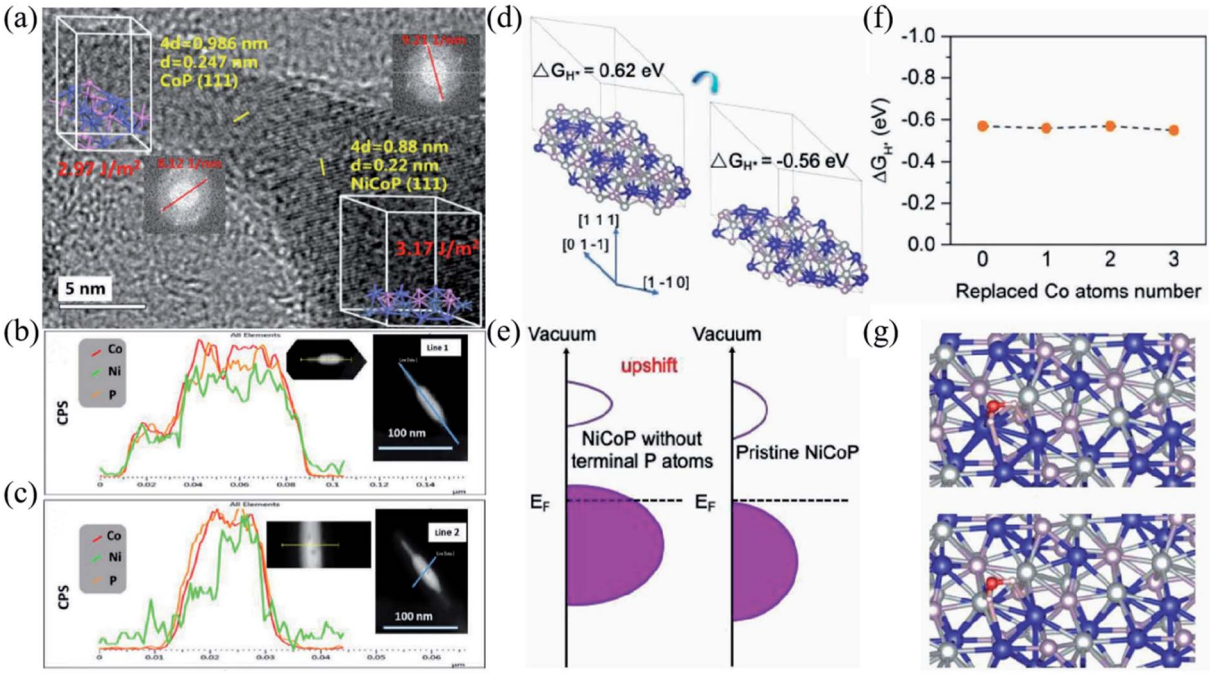

Fig. 10 (a) HRTEM image of CoP and NiCoP; the inset shows the calculated surface energies and fast Fourier transform. (b and c) Line scanning in different directions of CoP/NiCoP. (d) The optimized hydrogen atom adsorption structure. (e) The schematic on the projected density of states. (f) The ΔG_{H^+} values as the replaced Ni atoms increased. (g) The optimized hydrogen H_2O adsorption structure. Panels a–g adapted with permission from ref. 192, copyright 2019, WILEY-VCH.

 © 2021 The Author(s). Published by the Royal Society of Chemistry

Open Access Article. Published on 30 July 2021. Downloaded on 2/11/2026 5:52:39 PM. This article is licensed under a Creative Commons Attribution 3.0 Unported Licence.

surfaces of transition metal phosphides, their activity is better than that of other counterparts, such as carbides, nitrides, and sulfides.[186–188] Thus, transition metal phosphides are widely used in water decomposition, fuel cells, batteries, and supercapacitors.[189,190] Pang *et al.* prepared ultrathin and homogeneous 2D nickel–cobalt phosphate composite nanosheets, which are ultrathin enough to provide maximum mechanical flexibility and sufficient electroactive sites facilitating their electrochemical performance. The electrode shows a high specific capacity of 1132.5 F g^{-1} at 1 A g^{-1} and high rate performance with 63% capacity retention at 1 A g^{-1}.[191] Chen *et al.* built a nanoscale tadpole-like CoP/NiCoP heterojunction interface modulating the catalyst structure and thus strengthening the hydrogen precipitation and energy storage performance, as shown in Fig. 10a. Fig. 10b and c demonstrate linear sweeping in different directions, further revealing the elementary distribution of CoP/NiCoP. Density functional theory (DFT) explains the synergistic effect between NiCoP and CoP, confirming the effective proton adsorption/desorption ability of CoP/NiCoP (Fig. 10d). The d-band center of the H^+ capture site would shift upward from the Fermi energy level after the elimination of the terminal P atoms (Fig. 10e). After CoP loading, the coordination number of the Co–Ni shell layer in NiCoP would decrease, and some of the Ni atoms would be replaced by Co atoms on the surface. The magnitude of ΔG_{H^+} remains almost constant with the increased substitution of Ni atoms (Fig. 10f). In addition, the adsorption energy of H_2O (ΔE_{H_2O}) was calculated and is illustrated in Fig. 10g, which indicates that in the alkaline HER process the adsorption of H_2O would be improved and the dissociation is accelerated. The theoretical results show that the formation of the NiCoP/CoP heterojunction interface optimizes proton chemisorption and H_2O dissociation. The optimized phosphide crystal keeps the balance of the proton chemisorption and H_2O dissociation, thus accelerating the HER kinetics over a broad pH range. In addition, because of the unique properties, CoP/NiCoP had been proved as an excellent cathode material for SBHs with ultra-high rate performance, which was a specific capacity of 1106.2 F g^{-1} at 1 A g^{-1} and a specific capacity of 600 F g^{-1} at 100 A g^{-1}.[192]

4. Conclusion and outlook

As a new generation of energy storage devices, BSHDs with high energy density, power density, and cycling stability have a wide application prospect. Due to the poor conductivity and structural stability, and the slow ion diffusion kinetics, the rate performance of transition metal compound-based cathodes cannot meet the demand, limiting the practical application of BSHDs. To solve this problem, this review introduces the energy storage mechanism of BSHDs and summarizes some efficient strategies of reinforcing the rate performance of transition metal compound-based cathodes. It may put forward a reference for developing new strategies to further improve the rate performance of transition metal compound-based cathodes in BSHDs.

With respect to the future design and fabrication of BSHDs, a number of points are still worth considering; the corresponding outlooks are listed below:

4.1 Optimizing the experimental method

In the preparation of transition metal sulfide/selenide/phosphate, toxic gases such as H_2S, H_2Se and PH_3 may be produced, which are hazardous to human health. In addition, phosphorus-containing waste solution produced from the synthesis process needs to be carefully handled; otherwise it would cause environmental pollution. Therefore, the optimization of the preparation method is necessary.

4.2 Developing biomass-derived carbon materials

The complex synthesis process and high cost of graphene limit the wide application of transition metal compounds and graphene composites. Therefore, developing transition metal compound coupled biomass-derived carbon materials could be an effective strategy.

4.3 Amorphizing the surface

Amorphization is a process of making order crystals structurally amorphous. For electrode materials in SBHs, surface amorphization modulates the physicochemical properties, resulting in better electrochemical performance. Currently, most electrode materials are based on crystalline or layered compounds with good orderly crystallinity. However, a disorder part of the surface will be able to enhance the specific capacity of the material, and greatly increase the diffusion efficiency of ions, thus greatly improving the rate performance.[193]

4.4 Optimizing the electrolyte

Electrolyte is an important part of supercapacitors, whose interaction with the electrode would determine the electrode–electrolyte interface state, further having an impact on the rate performance. For example, aqueous electrolytes have high ionic conductivity, but are limited by low energy density and poor cycling stability. Organic electrolytes and ionic liquids usually have low ionic conductivity, although they can expand the potential window of electrode materials. Although water-in-salt electrolytes have a wide electrochemical window, making them promising electrolytes, their low conductivity and high viscosity limit their further application in SBHs. Therefore, there is a need for the design and development of more efficient electrolytes for SBHs.[194]

Author contributions

Cong Wang and Zehao Song wrote this manuscript; Pei Shi, Lin Lv, Houzhao Wan, Li Tao, Jun Zhang, Hanbin Wang, and Hao Wang supervised the work and revised the manuscript.

Conflicts of interest

We declare that we do not have any commercial or associative interest that represents a conflict of interest in connection with the work submitted.

Open Access Article. Published on 30 July 2021. Downloaded on 2/11/2026 5:52:39 PM.
This article is licensed under a Creative Commons Attribution 3.0 Unported Licence.

Acknowledgements

This work was supported by the National Natural Science Foundation of China (No. 52002122), the Science and Technology Department of Hubei Province (No. 2019AAA038), the Project funded by the China Postdoctoral Science Foundation (No. 2021M690947) and the Wuhan Yellow Crane Talent Program (No. 2017-02).

References

1 W. Xie, X. Jiang, T. Qin, H. Yang, D. Liu and D. He, *Electrochim. Acta*, 2017, **258**, 1064–1071.
2 W. Guo, C. Yu, S. Li, X. Song, H. Huang, X. Han, Z. Wang, Z. Liu, J. Yu, X. Tan and J. Qiu, *Adv. Mater.*, 2019, **31**, e1901241.
3 Y. Zhu, L. Peng, D. Chen and G. Yu, *Nano Lett.*, 2016, **16**, 742–747.
4 P. Xiong, R. Ma, N. Sakai, X. Bai, S. Li and T. Sasaki, *ACS Appl. Mater. Interfaces*, 2017, **9**, 6282–6291.
5 K. Ghosh, S. Ng, C. Iffelsberger and M. Pumera, *ACS Appl. Energy Mater.*, 2020, **3**, 10261–10269.
6 F. Wu, J. Chen, L. Li, T. Zhao and R. Chen, *J. Phys. Chem. C*, 2011, **115**, 24411–24417.
7 H. Nakanishi, I. Kikuta, H. Segawa, Y. Kawabata, R. Kishida, T. Norisuye and Q. Tran-Cong-Miyata, *ChemSusChem*, 2017, **10**, 701–710.
8 P. Cai, K. Zou, X. Deng, B. Wang, M. Zheng, L. Li, H. Hou, G. Zou and X. Ji, *Adv. Energy Mater.*, 2021, **11**, 2003804.
9 H. Qian, B. Wu, Z. Nie, T. Liu, P. Liu, H. He, J. Wu, Z. Chen and S. Chen, *Chem. Eng. J.*, 2021, **420**, 127646.
10 M. Akhtar, J.-K. Chang and S. B. Majumder, *J. Electrochem. Soc.*, 2020, **167**, 110546.
11 T. Nguyen and M. F. Montemor, *Adv. Sci.*, 2019, **6**, 1801797.
12 X. Zhang, W. Shi, J. Zhu, W. Zhao, J. Ma, S. Mhaisalkar, T. L. Maria, Y. Yang, H. Zhang, H. H. Hng and Q. Yan, *Nano Res.*, 2010, **3**, 643–652.
13 M. R. Das, A. Roy, S. Mpelane, A. Mukherjee, P. Mitra and S. Das, *Electrochim. Acta*, 2018, **273**, 105–114.
14 K. Dai, C. Liang, J. Dai, L. Lu, G. Zhu, Z. Liu, Q. Liu and Y. Zhang, *Mater. Chem. Phys.*, 2014, **143**, 1344–1351.
15 A. Roy, A. Ray, S. Saha, M. Ghosh, T. Das, B. Satpati, M. Nandi and S. Das, *Electrochim. Acta*, 2018, **283**, 327–337.
16 H. Mei, Z. Huang, B. Xu, Z. Xiao, Y. Mei, H. Zhang, S. Zhang, D. Li, W. Kang and D. F. Sun, *Nano-Micro Lett.*, 2020, **12**, 61.
17 S. Nandhini and G. Muralidharan, *J. Solid State Electrochem.*, 2020, **25**, 465–477.
18 Y.-Y. Chen, P. Dhaiveegan, M. Michalska and J.-Y. Lin, *Electrochim. Acta*, 2018, **274**, 208–216.
19 B. Xie, M. Yu, L. Lu, H. Feng, Y. Yang, Y. Chen, H. Cui, R. Xiao and J. Liu, *Carbon*, 2019, **141**, 134–142.
20 X. Zhang, A. Wu, X. Wang, C. Tian, R. An and H. Fu, *J. Mater. Chem. A*, 2018, **6**, 17905–17914.
21 Y. Lu, J.-P. Tu, Q.-Q. Xiong, J.-Y. Xiang, Y.-J. Mai, J. Zhang, Y.-Q. Qiao, X.-L. Wang, C.-D. Gu and S. X. Mao, *Adv. Funct. Mater.*, 2012, **22**, 3927–3935.
22 D. Yang, Z. Lu, X. Rui, X. Huang, H. Li, J. Zhu, W. Zhang, Y. M. Lam, H. H. Hng, H. Zhang and Q. Yan, *Angew. Chem., Int. Ed.*, 2014, **53**, 9352–9355.
23 J. Tian, Q. Liu, A. M. Asiri and X. Sun, *J. Am. Chem. Soc.*, 2014, **136**, 7587–7590.
24 M. K. Wu, C. Chen, J. J. Zhou, F. Y. Yi, K. Tao and L. Han, *J. Alloys Compd.*, 2018, **734**, 1–8.
25 N. Tang, W. Wang, H. You, Z. Zhai, J. Hilario, L. Zeng and L. Zhang, *Catal. Today*, 2019, **330**, 240–245.
26 Z. Xiao, L. Fan, B. Xu, S. Zhang, W. Kang, Z. Kang, H. Lin, X. Liu, S. Zhang and D. Sun, *ACS Appl. Mater. Interfaces*, 2017, **9**, 41827–41836.
27 H. Huang, H. Zhang, Y. Fan, X. Deng, G. Li, X. Liang, W. Zhou, J. Guo and S. Tang, *Appl. Surf. Sci.*, 2019, **481**, 1220–1227.
28 F. Liu, X. Chu, H. Zhang, B. Zhang, H. Su, L. Jin, Z. Wang, H. Huang and W. Yang, *Electrochim. Acta*, 2018, **269**, 102–110.
29 B. Huang, W. Wang, T. Pu, J. Li, J. Zhu, C. Zhao, L. Xie and L. Chen, *J. Colloid Interface Sci.*, 2018, **532**, 630–640.
30 M. Aghazadeh, A. Rashidi and M. R. Ganjali, *Electron. Mater. Lett.*, 2017, **14**, 37–45.
31 S. Li, N. Sharma, C. Yu, Y. Zhang, G. Wan, R. Fu, H. Huang, X. Sun, S. J. Lee, J. S. Lee, D. Nordlund, P. Pianetta, K. Zhao, Y. Liu and J. Qiu, *Adv. Mater.*, 2021, **33**, e2006147.
32 J. Zhao, B. Guan, B. Hu, Z. Xu, D. Wang and H. Zhang, *Electrochim. Acta*, 2017, **230**, 428–437.
33 J. Zhu, L. Xiang, D. Xi, Y. Zhou and J. Yang, *Bull. Mater. Sci.*, 2018, **41**, 54.
34 J. Ren, Q. Meng, Z. Xu, X. Zhang and J. Chen, *J. Electroanal. Chem.*, 2019, **836**, 30–37.
35 J. Li, Q. Li, J. Sun, Y. Ling, K. Tao and L. Han, *Inorg. Chem.*, 2020, **59**, 11174–11183.
36 T. Liu, J. Liu, L. Zhang, B. Cheng and J. Yu, *J. Mater. Sci. Technol.*, 2020, **47**, 113–121.
37 Y. Cui, J. Zhang, C. Jin, Y. Liu, W. Luo and W. Zheng, *Small*, 2019, **15**, e1804318.
38 L. Du, W. Du, H. Ren, N. Wang, Z. Yao, X. Shi, B. Zhang, J. Zai and X. Qian, *J. Mater. Chem. A*, 2017, **5**, 22527–22535.
39 J. Yang, Y. Yuan, W. Wang, H. Tang, Z. Ye and J. Lu, *J. Power Sources*, 2017, **340**, 6–13.
40 S. Xie, J. Gou, B. Liu and C. Liu, *J. Colloid Interface Sci.*, 2019, **540**, 306–314.
41 Y. Hu, C. Huang, S. Jiang, Y. Qin and H. C. Chen, *J. Colloid Interface Sci.*, 2020, **558**, 291–300.
42 P. Zhang, W. Wang, Z. Kou, J. Li, T. Wang and J. Guo, *Ionics*, 2021, **27**, 801–810.
43 Y. Gan, C. Wang, X. Chen, P. Liang, H. Wan, X. Liu, Q. Tan, H. Wu, H. Rao, H. Wang, J. Zhang, Y. Wang, P. A. van Aken and H. Wang, *Chem. Eng. J.*, 2020, **392**, 123661.
44 Y. Jin, C. Zhao, Q. Jiang and C. Ji, *Colloids Surf., A*, 2018, **553**, 58–65.
45 X. Zhang, L. Zhang, G. Xu, A. Zhao, S. Zhang and T. Zhao, *J. Colloid Interface Sci.*, 2020, **561**, 23–31.
46 J. Hei, L. Su, S. Chen, W. Ye, J. Zhan, L. Wang, Y. Gao, H. Wang and Y. Wang, *Part. Part. Syst. Charact.*, 2019, **37**, 1900344.

 © 2021 The Author(s). Published by the Royal Society of Chemistry

Open Access Article. Published on 30 July 2021. Downloaded on 2/11/2026 5:52:39 PM.
This article is licensed under a Creative Commons Attribution 3.0 Unported Licence.

47 P. Sun, Z. Li, L. Zhang, C. Dong, Z. Li, H. Yao, J. Wang and G. Li, *J. Alloys Compd.*, 2018, **750**, 607–616.
48 M. Gao, W.-K. Wang, X. Zhang, J. Jiang and H.-Q. Yu, *J. Phys. Chem. C*, 2018, **122**, 25174–25182.
49 Y. Song, X. Cai, X. Xu and X.-X. Liu, *J. Mater. Chem. A*, 2015, **3**, 14712–14720.
50 S. Yang, Y. Liu, Y. Hao, X. Yang, W. A. Goddard, 3rd, X. L. Zhang and B. Cao, *Adv. Sci.*, 2018, **5**, 1700659.
51 J. Chen, B. Luo, Q. Chen, F. Li, Y. Guo, T. Wu, P. Peng, X. Qin, G. Wu, M. Cui, L. Liu, L. Chu, B. Jiang, Y. Li, X. Gong, Y. Chai, Y. Yang, Y. Chen, W. Huang, X. Liu and M. Li, *Adv. Mater.*, 2020, **32**, e1905578.
52 Y. Cheng, J. Shu, L. Xu, Y. Xia, L. Du, G. Zhang and L. Mai, *Adv. Energy Mater.*, 2021, **11**, 2100026.
53 J. Xu and L. Wang, *Sci. Rep.*, 2019, **9**, 12557.
54 S. J. Arbaz, S. C. Sekhar, G. Nagaraju, B. Ramulu and J. S. Yu, *Adv. Mater. Technol.*, 2020, **6**, 2000793.
55 M. M. Baig, E. Pervaiz, M. Azad, Z. Jahan, M. B. Khan Niazi and S. M. Baig, *Ceram. Int.*, 2021, **47**, 12557–12566.
56 Z. Ma, Z. Sun, H. Jiang, F. Li, Q. Wang and F. Qu, *Appl. Surf. Sci.*, 2020, **533**, 147521.
57 X. Wei, Y. Zhou, X. Shen, J. Di, X. Wang and Q. Li, *Mater. Lett.*, 2021, **293**, 129636.
58 N. Parveen, A. I. Al-Jaafari and J. I. Han, *Electrochim. Acta*, 2019, **293**, 84–96.
59 Z. Tian, X. Wang, B. Li, H. Li and Y. Wu, *Electrochim. Acta*, 2019, **298**, 321–329.
60 S. Yang, Z. Han, F. Zheng, J. Sun, Z. Qiao, X. Yang, L. Li, C. Li, X. Song and B. Cao, *Carbon*, 2018, **134**, 15–21.
61 H. Chen, J. Jiang, L. Zhang, T. Qi, D. Xia and H. Wan, *J. Power Sources*, 2014, **248**, 28–36.
62 C. Wang, J. Wang, W. Hu and D. Wang, *Chem. Res. Chin. Univ.*, 2019, **36**, 68–73.
63 S. P. Gupta, M. A. More, D. J. Late and P. S. Walke, *Electrochim. Acta*, 2021, **366**, 137389.
64 X. Yang, J. Mao, H. Niu, Q. Wang, K. Zhu, K. Ye, G. Wang, D. Cao and J. Yan, *Chem. Eng. J.*, 2021, **406**, 126713.
65 J. Qian, X. Wu, Y. Cao, X. Ai and H. Yang, *Angew. Chem., Int. Ed.*, 2013, **52**, 4633–4636.
66 C. V. V. M. Gopi, S. Sambasivam, K. V. G. Raghavendra, R. Vinodh, I. M. Obaidat and H.-J. Kim, *Journal of Energy Storage*, 2020, **30**, 101550.
67 M. Zhang, Y. Xu, H. Fan, N. Zhao, B. Yan, C. Wang, J. Ma, A. K. Yadav, W. Zhang, Z. Du, X. Zheng, M. Li, G. Dong and W. Wang, *J. Alloys Compd.*, 2020, **826**, 154115.
68 J.-G. Seong, T. H. Ko, D. Lei, W.-K. Choi, Y.-S. Kuk, M.-K. Seo and B.-S. Kim, *Green Energy and Environment*, 2021, DOI: 10.1016/j.gee.2021.01.015.
69 Z. Cai, L. Deng, Y. Song, D. Li, L. Hong and Z. Shen, *Mater. Lett.*, 2020, **281**, 128626.
70 B. Kirubasankar, P. Palanisamy, S. Arunachalam, V. Murugadoss and S. Angaiah, *Chem. Eng. J.*, 2019, **355**, 881–890.
71 X. Wang, H. Yan, J. Zhang, X. Hong, S. Yang, C. Wang and Z. Li, *J. Alloys Compd.*, 2019, **810**, 151911.
72 Y. Lu, J. Liang, S. Deng, Q. He, S. Deng, Y. Hu and D. Wang, *Nano Energy*, 2019, **65**, 103993.
73 Q. Meng, K. Qin, L. Ma, C. He, E. Liu, F. He, C. Shi, Q. Li, J. Li and N. Zhao, *ACS Appl. Mater. Interfaces*, 2017, **9**, 30832–30839.
74 P. Cai, R. Momen, M. Li, Y. Tian, L. Yang, K. Zou, X. Deng, B. Wang, H. Hou, G. Zou and X. Ji, *Chem. Eng. J.*, 2021, **420**, 129647.
75 P. Sun, R. Wang, Q. Wang, H. Wang and X. Wang, *Appl. Surf. Sci.*, 2019, **475**, 793–802.
76 Y. Zhang, Y. Hu, Z. Wang, T. Lin, X. Zhu, B. Luo, H. Hu, W. Xing, Z. Yan and L. Wang, *Adv. Funct. Mater.*, 2020, **30**, 2004172.
77 K. Xiang, Z. Xu, T. Qu, Z. Tian, Y. Zhang, Y. Wang, M. Xie, X. Guo, W. Ding and X. Guo, *Chem. Commun.*, 2017, **53**, 12410–12413.
78 X. Wei, X. Jiang, J. Wei and S. Gao, *Chem. Mater.*, 2016, **28**, 445–458.
79 Z. Ge, Y. Zhang, D. Fu, L. He and M. Li, *Nano Select*, 2021, 1–10.
80 K. Liu, X. Zheng, K. Wang, C. Wang and M. Chen, *Carbon*, 2019, **153**, 265–273.
81 J. Tian, H. Zhang, Z. Liu, G. Qin and Z. Li, *Int. J. Hydrogen Energy*, 2018, **43**, 1596–1605.
82 L. Gu, Y. Wang, R. Lu, W. Wang, X. Peng and J. Sha, *J. Power Sources*, 2015, **273**, 479–485.
83 L. Long, Y. Yao, M. Yan, H. Wang, G. Zhang, M. Kong, L. Yang, X. Liao, G. Yin and Z. Huang, *J. Mater. Sci.*, 2016, **52**, 3642–3656.
84 F. Zhu, W. Liu, Y. Liu and W. Shi, *Chem. Eng. J.*, 2020, **383**, 123150.
85 S. Zhang, J. Wu, J. Wang, W. Qiao, D. Long and L. Ling, *J. Power Sources*, 2018, **396**, 88–94.
86 X. Yang, Y.-Y. Wang, B.-H. Hou, H.-J. Liang, X.-X. Zhao, H. Fan, G. Wang and X.-L. Wu, *Acta Metall. Sin.*, 2020, **34**, 390–400.
87 B. Dou, J. Yan, Q. Chen, X. Han, Q. Feng, X. Miao and P. Wang, *Sens. Actuators, B*, 2021, **328**, 129082.
88 Z.-Y. Gu, J.-Z. Guo, Z.-H. Sun, X.-X. Zhao, W.-H. Li, X. Yang, H.-J. Liang, C.-D. Zhao and X.-L. Wu, *Sci. Bull.*, 2020, **65**, 702–710.
89 R. B. Rakhi, W. Chen, M. N. Hedhili, D. Cha and H. N. Alshareef, *ACS Appl. Mater. Interfaces*, 2014, **6**, 4196–4206.
90 T. Dang, G. Zhang, Q. Li, Z. Cao, G. Zhang and H. Duan, *J. Colloid Interface Sci.*, 2020, **577**, 368–378.
91 P. Zhang, J. Zhou, W. Chen, Y. Zhao, X. Mu, Z. Zhang, X. Pan and E. Xie, *Chem. Eng. J.*, 2017, **307**, 687–695.
92 B. Tong, W. Wei, Z. Wu, L. Zhao, W. Ye, J. Wang, W. Chen, C. Soutis and L. Mi, *ACS Appl. Energy Mater.*, 2021, **4**, 3221–3230.
93 W. Sun, L. Xiao and X. Wu, *J. Alloys Compd.*, 2019, **772**, 465–471.
94 Y. Xiao, A. Dai, X. Zhao, S. Wu, D. Su, X. Wang and S. Fang, *J. Alloys Compd.*, 2019, **781**, 1006–1012.
95 B. Guan, Y. Li, B. Yin, K. Liu, D. Wang, H. Zhang and C. Cheng, *Chem. Eng. J.*, 2017, **308**, 1165–1173.
96 X. Ma, L. Zhang, G. Xu, C. Zhang, H. Song, Y. He, C. Zhang and D. Jia, *Chem. Eng. J.*, 2017, **320**, 22–28.

Open Access Article. Published on 30 July 2021. Downloaded on 2/11/2026 5:52:39 PM.
This article is licensed under a Creative Commons Attribution 3.0 Unported Licence.

97 W. Wang, L. Zhang, G. Xu, H. Song, L. Yang, C. Zhang, J. Xu and D. Jia, *Inorg. Chem.*, 2018, **57**, 10287–10294.
98 X. Lei, S. Ge, Y. Tan, Z. Wang, J. Li, X. Li, G. Hu, X. Zhu, M. Huang, Y. Zhu and B. Xiang, *ACS Appl. Mater. Interfaces*, 2020, **12**, 9158–9168.
99 A. Banerjee, S. Bhatnagar, K. K. Upadhyay, P. Yadav and S. Ogale, *ACS Appl. Mater. Interfaces*, 2014, **6**, 18844–18852.
100 L. Zhang, K. N. Hui, K. S. Hui, X. Chen, R. Chen and H. Lee, *Int. J. Hydrogen Energy*, 2016, **41**, 9443–9453.
101 L. Wang, X. Li, T. Guo, X. Yan and B. K. Tay, *Int. J. Hydrogen Energy*, 2014, **39**, 7876–7884.
102 S. Ji, Y. Ma, H. Wang, J. Key, D. J. L. Brett and R. Wang, *Electrochim. Acta*, 2016, **219**, 540–546.
103 M. Shi, M. Cui, L. Kang, T. Li, S. Yun, J. Du, S. Xu and Y. Liu, *Appl. Surf. Sci.*, 2018, **427**, 678–686.
104 Y. Tao, Y. Wu, H. Chen, W. Chen, J. Wang, Y. Tong, G. Pei, Z. Shen and C. Guan, *Chem. Eng. J.*, 2020, **396**, 125364.
105 J. Chen, Z. Xu, H. Zhu, R. Liu, X. Song, Q. Song, J. Wu, C. Zhang, L. Ding, J. Dong and H. Cui, *Vacuum*, 2020, **174**, 109219.
106 D. Guo, X. Song, F. Li, L. Tan, H. Ma, L. Zhang and Y. Zhao, *Colloids Surf., A*, 2018, **546**, 1–8.
107 Z. Liu, W. Zhou, S. Wang, W. Du, H. Zhang, C. Ding, Y. Du and L. Zhu, *J. Alloys Compd.*, 2019, **774**, 137–144.
108 Y.-Y. Huang and L.-Y. Lin, *ACS Appl. Energy Mater.*, 2018, **1**, 2979–2990.
109 S. C. Lee, S. Liu, P. A. Shinde, K. Y. Chung and S. Chan Jun, *Electrochim. Acta*, 2020, **353**, 136578.
110 P. Sivakumar, M. Jana, M. G. Jung, A. Gedanken and H. S. Park, *J. Mater. Chem. A*, 2019, **7**, 11362–11369.
111 X. Gao, X. Liu, D. Wu, B. Qian, Z. Kou, Z. Pan, Y. Pang, L. Miao and J. Wang, *Adv. Funct. Mater.*, 2019, **29**, 1903879.
112 J. Acharya, T. H. Ko, J.-G. Seong, M.-K. Seo, M.-S. Khil, H.-Y. Kim and B.-S. Kim, *ACS Appl. Nano Mater.*, 2020, **3**, 8679–8690.
113 F. Li, Z. Sun, H. Jiang, Z. Ma, Q. Wang and F. Qu, *Energy Fuels*, 2020, **34**, 11628–11636.
114 Z. Li, W. He, X. Wang, X. Wang, M. Song and J. Zhao, *Int. J. Hydrogen Energy*, 2020, **45**, 112–122.
115 N. Joseph, P. Muhammed Shafi and A. Chandra Bose, *New J. Chem.*, 2018, **42**, 12082–12090.
116 S. Kasap, I. I. Kaya, S. Repp and E. Erdem, *Nanoscale Adv.*, 2019, **1**, 2586–2597.
117 Y. Tang, H. Shen, J. Cheng, Z. Liang, C. Qu, H. Tabassum and R. Zou, *Adv. Funct. Mater.*, 2020, **30**, 1908223.
118 H. Liang, H. Jia, T. Lin, Z. Wang, C. Li, S. Chen, J. Qi, J. Cao, W. Fei and J. Feng, *J. Colloid Interface Sci.*, 2019, **554**, 59–65.
119 T. Xiong, M. Zhu, Y. Zhang, W. S. V. Lee, Z. G. Yu and J. Xue, *Batteries Supercaps*, 2020, **3**, 519–526.
120 Y. Guo, X. Hong, Y. Wang, Q. Li, J. Meng, R. Dai, X. Liu, L. He and L. Mai, *Adv. Funct. Mater.*, 2019, **29**, 1809004.
121 Y. Chen, D. Ni, X. Yang, C. Liu, J. Yin and K. Cai, *Electrochim. Acta*, 2018, **278**, 114–123.
122 J. Huang, J. Wei, Y. Xiao, Y. Xu, Y. Xiao, Y. Wang, L. Tan, K. Yuan and Y. Chen, *ACS Nano*, 2018, **12**, 3030–3041.
123 X. Liu, W. Zang, C. Guan, L. Zhang, Y. Qian, A. M. Elshahawy, D. Zhao, S. J. Pennycook and J. Wang, *ACS Energy Lett.*, 2018, **3**, 2462–2469.
124 J. Cao, J. Li, L. Li, Y. Zhang, D. Cai, D. Chen and W. Han, *ACS Sustainable Chem. Eng.*, 2019, **7**, 10699–10707.
125 X. Deng, K. Zou, R. Momen, P. Cai, J. Chen, H. Hou, G. Zou and X. Ji, *Sci. Bull.*, 2021, DOI: 10.1016/j.scib.2021.04.042.
126 D. H. Liu, W. H. Li, Y. P. Zheng, Z. Cui, X. Yan, D. S. Liu, J. Wang, Y. Zhang, H. Y. Lu, F. Y. Bai, J. Z. Guo and X. L. Wu, *Adv. Mater.*, 2018, **30**, e1706317.
127 M. Yang, Q. Ning, C. Fan and X. Wu, *Chin. Chem. Lett.*, 2021, **32**, 895–899.
128 T. Liu, L. Zhang, W. You and J. Yu, *Small*, 2018, **14**, e1702407.
129 A. M. Elshahawy, C. Guan, W. Zang, S. Ding, Z. Kou, S. J. Pennycook, N. Yan and J. Wang, *ACS Appl. Energy Mater.*, 2018, **2**, 616–626.
130 Y. Meng, P. Sun, W. He, B. Teng and X. Xu, *Nanoscale*, 2019, **11**, 688–697.
131 A. M. Elshahawy, C. Guan, X. Li, H. Zhang, Y. Hu, H. Wu, S. J. Pennycook and J. Wang, *Nano Energy*, 2017, **39**, 162–171.
132 Q. Li, H. Guo, R. Xue, M. Wang, M. Xu, W. Yang, J. Zhang and W. Yang, *Int. J. Hydrogen Energy*, 2020, **45**, 20820–20831.
133 P. Liu, M. Yang, S. Zhou, Y. Huang and Y. Zhu, *Electrochim. Acta*, 2019, **294**, 383–390.
134 T. Liu, C. Jiang, B. Cheng, W. You and J. Yu, *J. Power Sources*, 2017, **359**, 371–378.
135 T. Liu, L. Zhang, B. Cheng, W. You and J. Yu, *Chem. Commun.*, 2018, **54**, 3731–3734.
136 D. Zhang, X. Zhang, Y. Chen, C. Wang, Y. Ma, H. Dong, L. Jiang, Q. Meng and W. Hu, *Phys. Chem. Chem. Phys.*, 2012, **14**, 10899–10903.
137 S. Zhou, X. Jin, S. Zhu, Q. Luo, Z. Qiu, A. Wu and H. Huang, *Chin. Chem. Lett.*, 2020, **31**, 2353–2357.
138 C. Xiong, B. Li, X. Lin, H. Liu, Y. Xu, J. Mao, C. Duan, T. Li and Y. Ni, *Composites, Part B*, 2019, **165**, 10–46.
139 H. Yang, S. Kannappan, A. S. Pandian, J. H. Jang, Y. S. Lee and W. Lu, *Nanotechnology*, 2017, **28**, 445401.
140 W. Liu, K. Feng, Y. Zhang, T. Yu, L. Han, G. Lui, M. Li, G. Chiu, P. Fung and A. Yu, *Nano Energy*, 2017, **34**, 491–499.
141 Y. Zhang, Y. Shen, X. Xie, W. Du, L. Kang, Y. Wang, X. Sun, Z. Li and B. Wang, *Mater. Des.*, 2020, **196**, 109111.
142 U. Singh, A. Banerjee, D. Mhamane, A. Suryawanshi, K. K. Upadhyay and S. Ogale, *RSC Adv.*, 2014, **4**, 39875–39883.
143 H. Xing, W. He, Y. Liu, G. Long, Y. Sun, J. Feng, W. Feng, Y. Zhou, Y. Zong, X. Li, X. Zhu and X. Zheng, *ACS Appl. Mater. Interfaces*, 2021, **13**, 26373–26383.
144 A. Namdarian, A. G. Tabrizi, A. Maseleno, A. Mohammadi and S. E. Moosavifard, *Int. J. Hydrogen Energy*, 2018, **43**, 17780–17787.
145 S. Zhou, W. Wei, Y. Zhang, S. Cui, W. Chen and L. Mi, *Sci. Rep.*, 2019, **9**, 12727.
146 W. Luo, G. Zhang, Y. Cui, Y. Sun, Q. Qin, J. Zhang and W. Zheng, *J. Mater. Chem. A*, 2017, **5**, 11278–11285.

 © 2021 The Author(s). Published by the Royal Society of Chemistry

Open Access Article. Published on 30 July 2021. Downloaded on 2/11/2026 5:52:39 PM.
This article is licensed under a Creative Commons Attribution 3.0 Unported Licence.

147 Y. Yan, K. Li, X. Chen, Y. Yang and J. M. Lee, *Small*, 2017, **13**, 1701724.
148 P. Ji, J. Wan, Y. Xi, Y. Guan, C. Zhang, X. Gu, J. Li, J. Lu and D. Zhang, *Nanotechnology*, 2019, **30**, 335401.
149 K. Li, M. Liu, S. Li, F. Huang, L. Wang and H. Zhang, *J. Alloys Compd.*, 2020, **817**, 152712.
150 L. Wang, Y. Guan, X. Zhao, J. Mu, H. Che, H. Li and Z. Guo, *J. Mater. Sci.: Mater. Electron.*, 2018, **29**, 5782–5790.
151 W. Wei, J. Wu, S. Cui, Y. Zhao, W. Chen and L. Mi, *Nanoscale*, 2019, **11**, 6243–6253.
152 C. Wang, Z. Song, H. Wan, X. Chen, Q. Tan, Y. Gan, P. Liang, J. Zhang, H. Wang, Y. Wang, X. Peng, P. A. van Aken and H. Wang, *Chem. Eng. J.*, 2020, **400**, 125955.
153 N. Zhang, X. Li, T. Hou, J. Guo, A. Fan, S. Jin, X. Sun, S. Cai and C. Zheng, *Chin. Chem. Lett.*, 2020, **31**, 1221–1225.
154 S. Wu, H. Guo, K. S. Hui and K. N. Hui, *Electrochim. Acta*, 2019, **295**, 759–768.
155 R. K. Pandey, Y. Totake, S. Soh and H. Nakanishi, *ChemistrySelect*, 2019, **4**, 13543–13550.
156 J. M. Jeong, S. H. Park, H. J. Park, S. B. Jin, S. G. Son, J. M. Moon, H. Suh and B. G. Choi, *Adv. Funct. Mater.*, 2021, **31**, 2009632.
157 T. Peng, H. Wang, H. Yi, Y. Jing, P. Sun and X. Wang, *Electrochim. Acta*, 2015, **176**, 77–85.
158 X. Feng, Y. Huang, M. Chen, X. Chen, C. Li, S. Zhou and X. Gao, *J. Alloys Compd.*, 2018, **763**, 801–807.
159 X. Guo, W. Zhang, C. Qian, H. Yang and T. Fan, *Ceram. Int.*, 2018, **44**, 9696–9702.
160 B. Wei, H. Liang, Z. Qi, D. Zhang, H. Shen, W. Hu and Z. Wang, *Chem. Commun.*, 2019, **55**, 1402–1405.
161 Z. Hao, X. He, H. Li, D. Trefilov, Y. Song, Y. Li, X. Fu, Y. Cui, S. Tang, H. Ge and Y. Chen, *ACS Nano*, 2020, **14**, 12719–12731.
162 Y.-Y. Wang, B.-H. Hou, J.-Z. Guo, Q.-L. Ning, W.-L. Pang, J. Wang, C.-L. Lü and X.-L. Wu, *Adv. Energy Mater.*, 2018, **8**, 1703252.
163 J. Huang, Y. Xiong, Z. Peng, L. Chen, L. Wang, Y. Xu, L. Tan, K. Yuan and Y. Chen, *ACS Nano*, 2020, **14**, 14201–14211.
164 H. Xing, G. Long, J. Zheng, H. Zhao, Y. Zong, X. Li, Y. Wang, X. Zhu, M. Zhang and X. Zheng, *Electrochim. Acta*, 2020, **337**, 135817.
165 C. Zhang, C. Lei, C. Cen, S. Tang, M. Deng, Y. Li and Y. Du, *Electrochim. Acta*, 2018, **260**, 814–822.
166 X. Zheng, Y. Sun, S. Jin, K. Zhang, Y. Li, J. Yan, H. Qin and H. Ni, *Int. J. Electrochem. Sci.*, 2020, **15**, 6249–6256.
167 C. Lu, A. Li, T. Zhai, C. Niu, H. Duan, L. Guo and W. Zhou, *Energy Storage Mater.*, 2020, **26**, 472–482.
168 Y. Tian, J. Liu, X. Song, L. Zhao, P. Zhang and L. Gao, *Compos. Sci. Technol.*, 2020, **197**, 108263.
169 J. Ye, B. Hu, Y. Jin, Z. Wang, Y. Xi, L. Fang and Q. Pan, *Electrochim. Acta*, 2020, **349**, 136372.
170 Y. Ma, C. Hou, H. Zhang, Q. Zhang, H. Liu, S. Wu and Z. Guo, *Electrochim. Acta*, 2019, **315**, 114–123.
171 S. Mondal, U. Rana and S. Malik, *J. Phys. Chem. C*, 2017, **121**, 7573–7583.
172 J. Fu, J. Yun, S. Wu, L. Li, L. Yu and K. H. Kim, *ACS Appl. Mater. Interfaces*, 2018, **10**, 34212–34221.
173 I. Chakraborty, N. Chakrabarty, A. Senapati and A. K. Chakraborty, *J. Phys. Chem. C*, 2018, **122**, 27180–27190.
174 C. Pan, Z. Liu, W. Li, Y. Zhuang, Q. Wang and S. Chen, *J. Phys. Chem. C*, 2019, **123**, 25549–25558.
175 W. Bi, J. Wang, E. P. Jahrman, G. T. Seidler, G. Gao, G. Wu and G. Cao, *Small*, 2019, **15**, e1901747.
176 T. Hao, Y. Liu, G. Liu, C. Peng, B. Chen, Y. Feng, J. Ru and J. Yang, *Energy Storage Mater.*, 2019, **23**, 225–232.
177 Z. Gao, L. Zhang, J. Chang, Z. Wang, D. Wu, F. Xu, Y. Guo and K. Jiang, *Chem. Eng. J.*, 2018, **335**, 590–599.
178 Z. Gao, X. Liu, J. Chang, D. Wu, F. Xu, L. Zhang, W. Du and K. Jiang, *J. Power Sources*, 2017, **337**, 25–35.
179 K. Seevakan, A. Manikandan, P. Devendran, A. Baykal and T. Alagesan, *Ceram. Int.*, 2018, **44**, 17735–17742.
180 X. Long, Z. Zeng, E. Guo, X. Shi, H. Zhou and X. Wang, *J. Power Sources*, 2016, **325**, 264–272.
181 X. Zhao, H. Wan, P. Liang, N. Wang, C. Wang, Y. Gan, X. Chen, Q. Tan, X. Liu, J. Zhang, Y. Wang, H. Wang and H. Wang, *Nano Res.*, 2021, **14**, 2574–2583.
182 Y. Song, X. Zhao and Z.-H. Liu, *Electrochim. Acta*, 2021, **374**, 137962.
183 S. B. Kale, A. C. Lokhande, R. B. Pujari and C. D. Lokhande, *J. Colloid Interface Sci.*, 2018, **532**, 491–499.
184 N. Karthik, T. N. J. I. Edison, R. Atchudan, D. Xiong and Y. R. Lee, *J. Electroanal. Chem.*, 2019, **833**, 105–112.
185 S. Li, T. Chen, J. Wen, P. Gui and G. Fang, *Nanotechnology*, 2017, **28**, 445407.
186 F. Yang, J. Wang, S. Gao, S. Zhou and Y. Kong, *Mol. Catal.*, 2020, **486**, 110873.
187 X. Li, X. Xiao, Q. Li, J. Wei, H. Xue and H. Pang, *Inorg. Chem. Front.*, 2018, **5**, 11–28.
188 N. L. W. Septiani, Y. V. Kaneti, K. B. Fathoni, K. Kani, A. E. Allah, B. Yuliarto, Nugraha, H. K. Dipojono, Z. A. Alothman, D. Golberg and Y. Yamauchi, *Chem. Mater.*, 2020, **32**, 7005–7018.
189 P. Tian, Y. Wang, W. Li, S. Song, S. Zhou, H. Gao, H. Xu, X. Tian and J. Zang, *J. Catal.*, 2020, **382**, 109–120.
190 S. Ahmad, C. Yang, W. Xie, Z. Deng, H. Zhang, Y. Zhao and X. Su, *Carbon*, 2020, **158**, 912–921.
191 B. Li, P. Gu, Y. Feng, G. Zhang, K. Huang, H. Xue and H. Pang, *Adv. Funct. Mater.*, 2017, **27**, 1605784.
192 Y. Lin, K. Sun, S. Liu, X. Chen, Y. Cheng, W. C. Cheong, Z. Chen, L. Zheng, J. Zhang, X. Li, Y. Pan and C. Chen, *Adv. Energy Mater.*, 2019, **9**, 1901213.
193 T. Zhou, Y. Zheng, H. Gao, S. Min, S. Li, H. K. Liu and Z. Guo, *Adv. Sci.*, 2015, **2**, 1500027.
194 H. Liu, X. Liu, S. Wang, H.-K. Liu and L. Li, *Energy Storage Mater.*, 2020, **28**, 122–145.